

This is the final version of the book chapter submitted to the publisher. It does not include editorial and other minor changes, but is otherwise identical to the published version (post-print).

The authoritative version of this chapter is available from the publisher at DOI:10.1049/PBPO125G_ch5

Chapter 1

Offshore turbines with bottom-fixed or floating substructures

*Dr. Denis Matha¹ Dr. Frank Lemmer² and
Prof. Dr. Michael Muskulus³*

1.1 Introduction

1.1.1 Offshore Substructures

Wind turbines are applied offshore since 1991, when the first offshore wind farm in Vindeby, Denmark was commissioned. According to GEWEC, beginning of 2018 about 18,814 MW of offshore wind capacity has been installed, with the majority commissioned in the UK (6.8GW), Germany (5.4GW) and China (2.8GW). Recent auctions in Europe with subsidy-free winning bids mean that offshore wind can be produced economically at market-price, making offshore wind one of the most economic sources of renewable energy and it is expected that the capacity will grow to 100-120 GW by 2030.

Offshore wind turbine substructures can be generally categorized into two different types of foundations:

- **Bottom-Fixed Substructures**
The majority of fixed substructures are monopile and jacket substructures, which are steel structures fixed to the seabed by driven piles or suction buckets. Furthermore, gravity-based substructures made from concrete and steel tripod or tripile/multipile foundations have been built. While the depth ranges of both, monopiles and jackets is continuously extended due to novel monopile manufacturing techniques enabling pile diameters well above 10 m, and jackets in O&G applications having already been applied in water depths beyond 300m, there is a common understanding that beyond a depth of 50-80m, fixed structures will become less economic than floating foundations.
- **Floating Substructures**
Floaters are typically applicable in water depths beyond 40m. They are categorized in terms of how they achieve hydrostatic stability in pitch and roll. Shallow

¹Ramboll

²University of Stuttgart

³Norwegian University of Science and Technology NTNU

drafted (typical draft < 10 m) barge or ring-pontoon shaped structures are stabilized by the waterplane area; deep-drafted spar foundations (typical draft of > 70 m) achieve hydrostatic restoring in pitch and roll through their low center of gravity (achieved by heavy ballast at bottom of spar) relative to the center of buoyancy; tension leg platforms (TLP) are stabilized by the tendon system, i.e. the TLP hull has sufficient excess buoyancy to keep the tendons under tension in all conditions avoiding any slack line events. Column-stabilized semi-submersible designs (often three- or four-column designs with the wind turbine placed centrally or on one column) are stabilized by a hybrid combination of both waterplane area and ballast. Alternative configurations also are proposed, however they can all be categorized into the above.

1.1.2 General introduction into modelling of substructures in offshore wind

The uniqueness of this book is that the modeling and simulation challenge in each area is described with a holistic eye toward the integrated, multi-disciplinary nature of optimal wind plant design. As computational resources continue to expand, it is no longer essential to subdivide into highly granular modeling elements. Analysts can avoid inherent errors and inaccuracies that result from putting too much physics outside the individual model boundaries. Other texts, like [1], [2] or [3] are available that describe hydrodynamics in more detail, but this chapter is meant to provide guidance and insight into a systems perspective by clarifying interfaces between sub-systems. The section describes the inputs, outputs and boundary conditions for the substructure modeling area so that its integration into the overall system of the wind turbine and wind farm becomes clearer.

It is the opinion of the authors that progress in modeling and simulation for design will not only depend on ever-increasing accuracy within single disciplines and increasing computational performance enabling more detailed and higher discretized numerical analyses, but also depends on the multi-disciplinary understanding and broader modeling scope. Furthermore it shall always be considered, that in practise uncertainty in results is not only related to the accuracy of numerical models, but also to the model inputs (e.g. extrapolated extreme metocean conditions, which inherently are uncertain as they are based on past events) and the actual as-built system uncertainties (which are unknown during the design phase). This is the reason for application of safety factors in every technical design process, which are highly unlikely to be reduced even if simulation accuracy becomes highly accurate in certain fields. This section introduces relevant modelling interfaces, hydrodynamic load models, coupling schemes and discusses practical aspects. The next sections provide more detail on modelling aspects covering the description of ocean waves and associated wave models (1.2) and an explanation of the wave-structure interaction and hydrodynamic load models, as well as mooring system models (1.3). The chapter is concluded by a brief summary of the modelling limitations and an outlook (1.4).

1.1.3 Interfaces

For the offshore substructure, the physical boundary conditions are represented by the following interfaces:

- **Interface to the wind turbine tower:**
Typically for an offshore wind turbine this is the flange connection of the transition piece to the tubular steel tower. At this interface the loads from the wind turbine are introduced into the substructure. Wind turbine loads are discussed in a different chapter in this book in more detail.
- **Air-Substructure interface:**
Above seawater level, the substructure is influenced by aerodynamic wind loads, i.e. the surface pressure differences caused by turbulent wind. Due to the low elevation above sea level resulting in low wind speed (wind speed increases typically with a power or logarithmic law over height), typically these loads are relatively small compared to the rotor thrust loads and the wind loads on the tower. Aerodynamic aspects are presented in a different chapter in this book in more detail.
- **Water-Substructure interface:**
The loads acting from the water surrounding the substructure, in simple terms, are a result of the surface pressure and viscous shear forces generated by waves and currents interacting with the substructure (cf. Navier Stokes equation). From a macroscopic viewpoint, the metocean conditions, i.e. the incident waves and currents, are usually driven by wind and tidal effects, and possibly also by seismic events. The ocean wave spectrum is dominated by wind generated waves accounting for more than half of the energy carried by all waves at the surface, surpassing the contribution of tides, tsunamis, coastal surges, and other factors. There are two types of wind generated waves at the ocean surface, wind seas and swell waves. As waves propagate away from their generation area, or when their phase speed overcomes the local wind speed, the result is called swell. These waves can travel long distances across the globe. Wind seas are generated locally and are strongly coupled to the local wind field; swells are generated remotely and are not directly coupled to the local wind field. Currents consist of wind and tidal contributions.
The presence and relative motion of the substructure itself also influences the pressure in the surrounding fluid (radiation and diffraction). The resulting hydrostatic and hydrodynamic loads are described in more detail in the following sections.
- **Soil-Substructure interface**
At the piles or anchors, the contact of the substructure with the surrounding soil is a key interface particularly for the design of fixed structures, as it is the final interface into which the loads from wind and waves acting on the wind turbine are transferred to (some energy is dissipated into the fluid as well, particularly for floaters). In the context of soil-pile/anchor or soil-mooring line interaction, geotechnical considerations are highly relevant. The resistance from the soil to vertical and lateral forces is dependent on the stratification, material and density

of the soil layers, as well as the cyclic loads exerted onto the soil from the wind turbine. Geotechnical aspects are presented in a different chapter in this book in more detail.

Designing offshore fixed or floating substructures for wind turbines requires modelling of all relevant external loads at the above interfaces, i.e. compared to onshore wind turbines additional loads from wind, waves and currents need to be represented. Furthermore, the interaction of the piles, anchors or mooring lines with the surrounding water, soil and seabed must be considered. Additional challenges and considerations for the design and optimization of support structures for fixed-bottom turbines and floaters have been discussed in the literature [4, 5].

1.1.4 Modelling of hydrodynamic loads

This chapter focuses on the numerical modelling of hydrodynamic loads on the substructure and mooring system. Figure 1.1 presents schematically how the design-relevant loads on the substructure from the external environmental conditions are typically modelled. In principle, the inputs and outputs to the force/loading models are:

- System parameters
 - Mass
 - Geometry (i.e. wetted surface geometry, water depth/bathymetry)
 - Material properties (i.e. stiffness, damping)
- Environmental conditions
 - Wave conditions, usually described by a one- or two-peaked wave spectrum (parameterized by peak spectral periods and shape parameters, scaled by a significant wave height) and information about its directionality
 - Current conditions, usually represented by a separate wind generated component, conditioned on the wind speed, and a tidal generated component varying with the rise and fall of the tide, both with a current profile over water depth and directionality information.
 - Water level changes from tides and storm surges
- Simulation outputs
 - Pressures/sectional forces/moments on and stresses within the substructure
 - Elastic deformations and rigid body motions of the substructure or moorings

On the left-hand side of the figure, the input for the metocean wave and current conditions is provided by a spectrum. The spectrum is parametrized for the specific site conditions by defining the free surface boundary conditions in terms of significant wave height and peak spectral period. Under consideration of the water depth, a wave model is applied to describe the seaway, i.e. enabling the derivation of fluid kinematics and pressures. The wave models used are usually potential flow theory based linear or higher order models, with the higher order models being more relevant for extreme wave events and shallow water locations due to their ability to better describe nonlinear steep waves common in such conditions.

With the knowledge of the substructure's wetted surface geometry and the wave model's outputs, the hydrodynamic force models can be applied to compute the forces on the substructure and moorings. The force models can generally be categorized into semi-empirical models such as Morison equation (using wave kinematics as an input, empirically considering viscous effects by drag coefficients), potential flow models (accounting for hydrostatics, radiation and diffraction forces, but without consideration of viscous effects) or Navier-Stokes based models such as Reynolds-averaged Computational Fluid Dynamics (CFD) approaches, typically using one- or two-equation turbulence models. The linear force models can be applied in both frequency and time domain, while the higher order force models can only be solved in the time-domain, involving the integration of every term of the governing differential equations over a time step.

Most widely used modeling techniques for fixed and floating bodies can be categorized into those assuming a "transparent" substructure, and those modeling the effect the substructure has on the wave field. The undisturbed wave kinematics over depth can be calculated through potential flow approaches giving analytical formulations. When it comes to the second approach, representing the impact of the substructure on the wave field, the Boundary Element Method (BEM) is applied in computer programs that solve for either the pressure on a fixed body in the domain (diffraction problem), or for the pressure on a moving body in response to its own motion (radiation problem).

The outputs from these force models are pressures, respectively forces acting on the substructure and mooring line elements. The structural dynamics of the substructure are usually modelled by approaches based on rigid body (still often applied for floaters) mechanics, beam-based truss representations, or finite shell or volume element models. Often these different levels of structural models are also applied in global-local cascading modelling schemes, where initially loads on the global model are calculated (e.g. a rigid or beam based model), and the local details are designed in a sequential step using the global loads applied onto a local finite element (FE) model. The structural model responds to the forces by determining structural stresses, elastic deflections and rigid body motions, which is fed-back into the hydrodynamic load model in terms of positions and velocities. The positions and velocities at structural interface nodes are also transferred to the soil and wind turbine models (addressed in other chapters).

1.1.5 Coupling Schemes

As evident from the introduction, various models for the different load contributions, as well as the structural representation of the substructure exist. The coupling of these different force and structural models, i.e. how loads and motions are exchanged between different models and domains, is a numerically challenging problem: In general the applied coupling schemes are classified in terms of physical single and multi-field problems, also generically called partitions. A second classification is in terms of the spatial dimensions of the coupling. For substructure problems, the coupling is always a surface problem where the two fields only interact

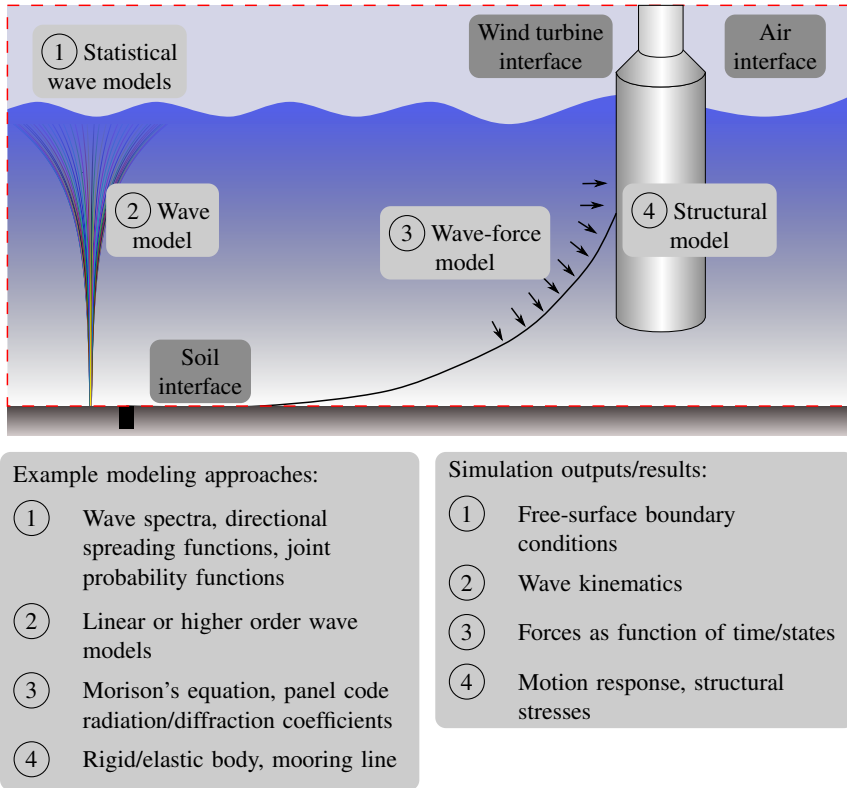


Figure 1.1 Hydrodynamic Modeling of the Offshore Wind Turbine System.

on their common surface, such as the wetted hull surface. In contrast, volume problems with overlapping fields as in case of porous materials or electrical problems are usually not present, if neglecting soil processes (with its two main manifestations, liquefaction and erosion) as commonly done. The third classification is regarding time integration methods used. Here implicit and explicit algorithms are used. Implicit algorithms (e.g. backward Euler integration) require information of the current state and the state in the next timestep (necessitating iteration), whereas explicit algorithms (e.g. forward Euler, Runge-Kutta schemes) require only data from the states of the current timestep to advance the solution.

In substructure modelling, two approaches are most relevant: (1) monolithic and (2) partitioned schemes.

The monolithic (or simultaneous) treatment combines all physical and computational fields into one system. Outcome is one specialized system of PDEs discretized over the whole domain which is solved with one integrator. All interactions are accurately modelled and the stability of the system is high. Problems of this approach are that different characteristic properties such as different time and spatial-scales (meteorological large scale turbulence vs. airfoil boundary layer flow) cannot be treated in

an optimized manner leading to greater complexity and typically smaller required timestep sizes and higher resolution domain discretizations, ultimately leading to higher resulting computational time. Also dedicated monolithic programs for each specific problem must be developed where a small change in FOWT design could require a new code development. For integrated FOWT (and general WT) simulation no pure monolithic approach has been developed until now except for simple reduced models for control design purposes neglecting many important physical effects; but recent developments allow for that option. In the past years, CFD models have been applied by a number of researchers (see e.g. [6]) modelling both the air and water in a monolithic CFD model (however, not accounting for the wind driving the waves), with the resulting loads being applied to a beam or FE based structural model.

Partitioned treatment is characterized by modelling the separate fields computationally independently using separate integrators with their own time steps. The interaction of the fields is ensured by communicating coupling quantities. Continuity, stability and accuracy must be ensured through careful implementation and formulation. The advantage of this treatment is the possibility of great customization and optimization of the independent modelling in each field facilitating also modularity and flexibility in the modules used in each field. It also becomes possible to separately model different structural components such as turbine rotor and support structure [7]. Existing methods and software can be easily reused and also industry-confidentiality-friendly black-box solutions are possible. These advantages led to offshore wind turbine designers using partitioned methods to simulate the system. This treatment is typically applied for the hydrodynamic coupling of the below presented load models with the structural models.

1.1.6 Practical modelling challenges

While in principle a range of simplified and advanced modelling methodologies exist to simulate offshore wind turbines, there are a number of practical limitations and constraints, which need to be considered in commercial projects. These can be summarized into limited availability of data due to missing site data and restrictions related to data exchange and confidentiality, the split of commercial projects into different design phases with tight time restrictions, and the commercial availability of computational resources and suitable software.

Currently, the design of Floating Offshore Wind Turbines (FOWTs) builds on the existing and established methodologies for onshore wind turbines on the one side and on the procedures for offshore structures on the other side. An overview of the current design process for fixed-bottom offshore turbines in comparison to floating turbines is provided in the paper [8] and the related project report [9]. In that paper an example is given where the fixed-bottom substructure and the turbine were designed based only on a limited exchange of system parameters between the two designers.

Consequently, no integrated design is performed but only load calculations with approximate or simplified models, delivered by the supplier. What does this imply?

On the one side it means that the structural dimensioning of offshore wind turbines follows proven and certified procedures and the systems satisfy risk and safety regulations. On the other side however, the confidentiality policy impedes full-system optimizations. Especially for the new technology of FOWTs it is important to save costs at early stages of the design process as a large portion of upcoming lifecycle costs is committed already at the beginning of the design process, see [10, p. 44]. The technological and market state for FOWT reported in [10] names the challenges due to intellectual property and the need for collaborative research, and highlights on the other side the large potential for cost reduction related to the platform size [10, p. 143]. Despite the problems related to proprietary data it is the task of research to address the potential of an integrated design methodology and the potential for cost reduction towards a sustainable offshore wind technology. However, not only confidentiality is an issue, but also practical availability of site specific data such as metocean and soil reports is often limited, particularly in the early design stages. Also, the wind turbine is often not selected at early design stages, requiring generic assumptions. Therefore, often the database is simply not present to feed highly detailed models with sufficient data to obtain more accurate results.

The project time constraints result in further challenges: In [9] the first out of three design stages includes mainly so-called spreadsheet calculations, but no simulation studies of the entire FOWT system — often also related to the above mentioned limited availability of site data or information on the wind turbine. After this stage, however, many decisions are taken and the design is being frozen. Therefore, design tools of “medium-fidelity” are important to enable designers to run comprehensive sensitivity and optimization studies already during the conceptual design phase establishing the basis for the decision-making in the subsequent phase.

While often solutions for advanced and highly accurate methods exist, availability of computational resources and software is also limiting their application in practise. This is why e.g. CFD in offshore wind applications is only applied in an industrial context to very specific problems, such as wave run-up analyses on secondary structures such as boat landings. A more extensive application of CFD to a wider range of load cases is limited by the high computational demands as well as the challenges in robust and reliable a-priori tuning of the CFD model parameters without availability of measurements (particularly turbulence models are very sensitive to grid quality, discretization or surface roughness and other parameters that can significantly influence the results).

1.2 Ocean wave modelling

The aim of numerical wave models is to determine the sea surface elevation and water particle velocities that are needed to estimate wave forces. Wave modelling can take place on different length scales, ranging from global circulation models (typically coupled with an atmospheric model) to local models used for detailed wave condition modelling at one specific site of interest, e.g., a single turbine. In between lie regional models that resolve local wave conditions in an area of interest,

e.g., containing a planned wind farm. The level of detail typically increases with decreasing scale due to computational limitations at larger scales.

A first distinction can be made between depth-averaged and depth-resolving models. Whereas depth-resolving models simulate the full 3D water volume, depth-averaged models do not resolve vertical water transport and focus on the vertically integrated wave energy or sea surface profile only. This makes this class of models unsuitable for global ocean modelling where vertical currents play an important role.

The main application of depth-averaged models is to resolve large-scale wave motion in deep waters and to provide far-field information as input for more detailed wave models. The most common approach for large-scale wave modelling are spectral models such as WAM [11] or WaveWatch III [12]. These models simulate the energy transfer between wave frequency components due to nonlinear wave-wave interaction, white capping and reflection on coastlines or groups of islands, and the generation of waves by wind. The SWAN model [13] also includes current-wave interaction, dissipation due to bottom friction on sandy bottoms in the continental shelf, and wave breaking processes in the coastal near-zone, and is therefore suited for coastal applications [14]. However, as no phase information is retained, these models cannot resolve phase-dependent wave diffraction, so the detailed wave pattern around structures in the coastal zone cannot be correctly determined.

More details can be resolved with wave models based on the mild-slope equations [15] that can more accurately account for (mildly) varying sea bottom profiles, but these are restricted to linear waves. Therefore, these models can only determine wave conditions at a nearshore location where wave nonlinearity is not too strong.

In cases where nonlinear, steep waves or very shallow seas need to be considered, the Boussinesq model and its various extensions is a phase-resolving depth-averaged model that offers high spatial resolution. Waves in deep seas can be accurately described by linear wave theory. Waves in extremely shallow waters can be described by shallow water equations. The Boussinesq equations cover the middle ground, from intermediate water depths to shallow waters and can include terms to represent wave breaking. Therefore these models have been included in commercial coastal engineering software (e.g. MIKE21 by Danish Hydraulic Institute (DHI)) and are currently an active area of research regarding their application to wind farm design and siting.

Depth-resolving models solve the 3D Navier Stokes equations and have two application areas. For global circulation modelling the solution procedure is highly simplified and quasi-three-dimensional hydrostatic pressure models are used (e.g. Princeton Ocean Model [16]). The other application area is detailed modelling of complex wave problems, such as flow around non-trivial structures (e.g. a gravity-base wind turbine), flow-structure-interaction with a floating wind turbine, the determination of wave slamming events, or the simulation of critical offshore operations (e.g. wind turbine installation). Used with a suitable turbulence model, these models are what is commonly meant by the “CFD approach” to water wave modelling. Without a turbulence model, the models are known as potential flow models. This latter class of models is able to simulate highly nonlinear waves in both deep and shallow waters, but is not able to simulate breaking waves or the interaction with

small bodies or structural details, during which viscous effects play a major role. It is these last two classes of models which are mainly of interest in this chapter.

In practice, ocean waves can be separated into linear surface waves with a sinusoidal profile and steeper waves with a profile of relatively larger troughs and comparably shorter crests. Different wave theories exist to model the kinematics of such waves. Usually potential flow theory is employed with different orders of non-linearity of the free surface, see [17, p. 75] for a visualization of the different regimes. Linear waves can be modeled in a straightforward manner with potential flow theory. If no obstacles in the domain are considered, the wave kinematics can be solved for explicitly, see e.g. [3, p. 5-12]. The remainder of this section focuses on the left column of Figure 1.1, the free surface modeling and the determination of wave kinematics for a single wind turbine, while fluid-structure interaction is the subject of Section 1.3.

1.2.1 *Statistical descriptions*

A wave spectrum is a convenient way to describe the wave conditions at a site (in not too shallow waters), and is a typical output of large scale wave modelling, as discussed above, or from on-site measurements with a wave buoy. This reflects the empirical fact that the wave elevation process is approximately a Gaussian random process, at least for not too steep waves [18], fully characterized by its autocorrelation function.

The spectrum is the Fourier transform of the autocorrelation function, and can be understood as a frequency decomposition of the variance of the underlying stochastic process. Given a spectrum, it is possible to construct synthetic time series with the same spectral properties. The standard approach is to sum up a large number of discrete frequency components with random phases and amplitudes chosen proportional to the (square root of the) spectral power density at those frequencies [19].

1.2.2 *Potential flow models*

The basic equations of fluid flow for an incompressible fluid are the Navier Stokes equations, given in terms of the fluid velocity vector u , as

$$\nabla \cdot u = 0 \tag{1.1}$$

$$\frac{\partial u}{\partial t} + u \cdot \nabla u = -\frac{1}{\rho} \nabla p + g + \nu \nabla^2 u. \tag{1.2}$$

The first equation is the continuity equation. The second equation is the momentum equation. Its left hand side is the total derivative of the fluid (the sum of the local and the convective acceleration), the right hand side sums up the forces acting on the fluid particles. These consist of pressure forces, body forces due to gravity, and viscous forces. Here ρ denotes the density of the fluid, p is the pressure, and ν is the kinematic viscosity.

Strictly speaking, sea water is a viscous fluid, and the motion of the fluid in the sea is subject to internal viscous dissipation and viscous effects at the sea surface

and seabed (and other boundaries, such as immersed structures). Viscous effects are typically limited to a thin boundary layer, however, so the motion of the main body of water is often irrotational. It can therefore be described by a scalar velocity potential φ , which is a considerable mathematical simplification, as the water particle velocities u are then given by the gradient

$$u = -\nabla\varphi. \quad (1.3)$$

The continuity equation can then be written

$$\nabla \cdot u = \nabla(-\nabla\varphi) = -\nabla^2\varphi = 0, \quad (1.4)$$

which is the Laplace equation for the velocity potential. Fluid flow that occurs as a solution to this equation is called potential flow. Since the Laplace equation can be solved more efficiently than the full Navier Stokes equations, this is the traditionally most common way to resolve the wave kinematics for engineering applications.

The relationship between fluid pressure and velocity potential is given by the Bernoulli equation. Its general form reads

$$-\frac{\partial\varphi}{\partial t} + \frac{1}{2}\nabla u \cdot \nabla u + \frac{p}{\rho} + gz = C(t), \quad (1.5)$$

where $C(t)$ is an integration constant depending on boundary conditions.

1.2.3 Linear wave theory

The Laplace equation (1.4) is linear and can be solved analytically in certain cases. The most useful case occurs when the boundary conditions are linearized, which leads to linear wave theory, also called Airy or small-amplitude wave theory. Assuming that the velocity potential is periodic both in time (with period T) and space (with wavelength L), the solution is

$$\varphi = -\frac{H}{2} \frac{g}{\omega} \frac{\cosh k(h+z)}{\cosh kh} \sin(kx - \omega t), \quad (1.6)$$

for constant water depth h (see e.g. [20] for a detailed derivation). Here $H = 2a$ is the wave height (twice the wave amplitude a), $\omega = 2\pi/T$ is the wave angular frequency, and $k = 2\pi/L$ is the wave number. The vertical coordinate z is zero at the mean sea level and negative inside the water column. This leads to a free surface displacement

$$\eta = \frac{H}{2} \cos(kx - \omega t), \quad (1.7)$$

and water particle velocities and accelerations can be readily calculated as well. Note that the approximation is based on the assumption that both the wave steepness ka and the relative wave amplitude a/h are small. Simplification of the hyperbolic depth-dependence in (1.6) is possible for short waves ($kh \gg 1$), the so-called deep water limit, or for long waves ($kh \ll 1$), the so-called shallow water limit. The resulting formulas are not repeated here, but can be found in any standard monograph on hydrodynamics (e.g. [21]).

When predicting wave forces from linear theory, one complication is that the formulas for water particle velocity predict unrealistic values above the mean sea

level. The empirical correction by Wheeler [22] addresses this by stretching the potential to an effective height $zd/(\eta + d)$, so that

$$\phi = -\frac{H}{2} \frac{g}{\omega} \frac{\cosh k \left(h + z \frac{d}{\eta + d} \right)}{\cosh kh} \sin(kx - \omega t), \quad (1.8)$$

where η is the instantaneous sea surface elevation.

1.2.4 Frequency domain representation

Linear wave theory allows for the use of frequency domain calculations, which is attractive due to their high efficiency. Especially when calculating the entire system in the frequency large improvements in terms of computational speed can be achieved, see [23] and [24].

Linear waves travel with the phase speed v_p , which is a function of the wave frequency. The dispersion relation $\omega^2 = gk \tanh kh$ established the connection between the behavior in time and the spatial dimension of linear waves. For deep waters with a depth-to-wavelength ratio $h/\lambda > 1/2$ it can be simplified to $\omega^2 = gk$, leading to the phase speed

$$v_p = \frac{1}{2} \sqrt{\frac{g}{k}} = \frac{1}{2} \sqrt{\frac{g\lambda}{2\pi}} \quad (1.9)$$

where k denotes the wavenumber, see [2, Chapter 6.2].

The incident wave time series at different locations along the wave direction x can be represented as function of the wavenumber k with the factor e^{ikx} in the frequency-domain.

The wave kinematics over depth z can now be calculated from the amplitude spectrum of the wave height $A_\zeta(\omega)$. This results from the square root of the power spectrum $S_{\zeta\zeta}(\omega)$ with a scaling, dependent on the discretization. The kinematics, with the water particle velocity and acceleration in both horizontal and vertical direction, are necessary for the calculation of the wave forces through Morison's equation. In the frequency-domain the velocity calculation results in

$$v_x(\omega, x, z) = \omega A_\zeta(\omega, x) e^{kz} \quad (1.10)$$

$$v_z(\omega, x, z) = i\omega A_\zeta(\omega, x) e^{kz}, \quad (1.11)$$

where $A_\zeta(\omega, x)$ denotes the instantaneous wave elevation amplitude spectrum. Consequently, the horizontal velocity is in phase with the instantaneous free-surface elevation ζ_x , while the vertical velocity is 90 degrees ahead of the free-surface elevation. The water particle acceleration can be written as

$$a_x(\omega, x, z) = \omega^2 A_\zeta(\omega, x) e^{kz} \quad (1.12)$$

$$a_z(\omega, x, z) = -\omega^2 A_\zeta(\omega, x) e^{kz}. \quad (1.13)$$

If obstacles are present in the computational domain, e.g. fixed or floating bodies, the dimensions of the body determine the characteristics of the wave-induced

forcing. Potential flow can model effects from diffraction (of the waves around the floating body) as well as the forces from radiated waves acting back on the body. Viscous loads, on the other side, are entirely neglected by potential flow theory. This is the strength of the empirical Morison equation, addressed later in this section.

1.2.5 Nonlinear wave theories

A straightforward extension of the small amplitude wave theory is to solve the potential flow equation while keeping higher order terms in the boundary conditions. This perturbative approach results in the so-called Stokes wave theory of order n , when terms up to n -th order are retained. For example, the second-order sea surface displacement is (assuming that the mean sea level is zero),

$$\eta = \frac{H}{2} \cos(kx - \omega t) + \frac{H^2 k}{16} \frac{\cosh kh}{\sinh^3 kh} (2 + \cosh 2kh) \cos 2(kx - \omega t). \quad (1.14)$$

The validity of the different Stokes wave theories is mainly governed by requirements on the convergence of the perturbation expansion. A typical criterion is that the wave should have a single crest, which leads to restrictions on the maximum wave height for which Stokes theory remains valid.

The Stokes approach becomes quite involved for higher orders, and in practice orders above fifth are seldom used. An alternative that is computationally more advantageous is stream function wave theory [25]. Using the stream function, the water wave problem automatically satisfies the kinematic free surface boundary condition. It is assumed that the stream function has the form

$$\Psi(x, z) = Cz + \sum_{n=1}^N X_n \sinh(nk(h+z)) \cos nkx. \quad (1.15)$$

The coefficients X_n of the n -th order stream function need to be determined by an iterative procedure that is easily implemented on a computer. However, a stream function only exists for two-dimensional problems, in general, so the method is only applicable to model long-crested (planar) waves.

Finally, we briefly mention cnoidal wave theory, which is a shallow water wave theory with periodic waves. The sea surface displacement is developed in terms of Jacobian elliptic integrals $cn(u)$. Although well suited to shallow water, it seems that stream function theory can provide an even better fit to the sea surface, if a sufficiently high order is used.

1.2.6 Computational fluid dynamics approaches

In cases where detailed wave-structure interaction needs to be resolved, numerical methods based on solving the underlying PDEs are typically employed. As this is a highly specialized area, we only mention the main approaches and refer the reader to the dedicated literature (e.g. [26]).

A distinction can be made between mesh-based and mesh-less methods. Mesh-based methods discretize the spatial domain into a number of connected elements or cells. The finite difference method (FDM) is the most straightforward and ap-

proximates the derivatives of the underlying PDE at the nodes of the mesh by a finite difference scheme. The finite volume method (FVM) can be seen as the integral formulation of the FDM over a small control volume around each node and has a similar formulation. Popular high-order schemes for solving the convection equation in these approaches are the Crank-Nicolson implicit method using a sparse matrix solver, and the Lax-Wendroff explicit method. Numerical oscillations are suppressed by numerical damping using the first order upwind scheme or an alternative. The finite element method (FEM) is similar, but approximates the solution to the PDE instead of the equations themselves.

The main computational challenge with the Navier Stokes equations is the determination of the pressure. As the pressure depends on the velocity field, it is necessary to solve the Poisson equation $\nabla^2 p = -f(u)$, which involves the solution of a large sparse matrix equation. Various methods have been developed to increase the efficiency of the pressure determination, e.g. the SIMPLE and PISO algorithms.

Another computational challenge is the tracking of the free surface. Two popular approaches are the VOF method [27] that tracks the density in each cell, and the more recent level set method [28] that tracks the evolution of a level set function ψ which is zero on the interface boundary.

A turbulence model is needed to represent viscous processes. For engineering purposes, the Reynolds stress model is typically used, resulting in Reynolds-averaged Navier Stokes (RANS) equations. Various ways exist to model the Reynolds stresses, the most commonly used are simple one- or two-equation models such as the Spalart and Allmaras model [29] or the $k - \epsilon$ model. More recently, large eddy simulation (LES) has been used that applies a spatial filter to the Navier Stokes equations and uses a subgrid scale model to resolve the effect of turbulence below the modelled scale, e.g. based on the eddy viscosity concept.

Commercial software that implements the above methods (typically the FVM or the FEM) is readily available in general-purpose multi-physics simulation packages such as ANSYS/FLUENT or STAR-CD. Direct numerical solution (DNS) of the NSE without application of turbulence models implies that the whole range of spatial and temporal scales of the turbulence must be resolved, requiring an extremely refined computational mesh. Therefore, the computational cost of DNS is very high, even at low Reynolds numbers and typically DNS is only applied for fundamental research problems such as turbulent boundary layer problems using supercomputers.

For solving the Laplace equation in potential flow problems, the BEM is popular. It is based on reducing the volume integration into a surface integration, reducing the dimension of the problem by one. The traditional software implementing the BEM for water wave problems has been WAMIT, but more recent alternatives include ANSYS AQUA and the open-source code NEMOH.

An example of a mesh-less method is smoothed particle hydrodynamics (SPH), that approximates the solution of the PDE by a number of Lagrangian particles [30].

1.2.7 *Breaking waves*

Wave breaking is the process by which high waves become unstable and collapse. It is an important process by which waves transform excess energy into turbulence and

occurs naturally in deep and intermediate water, when the critical wave height $H_b = \frac{1}{7}L \tanh kh$ is exceeded. In shallow water, the criterion is based on the ratio of wave height to local water depth, e.g. in the classical $H_b = 0.78h$ criterion [31]. Breaking waves in shallow water occur in different types that have different implications for the design of structures. The surf similarity parameter

$$\xi_b = \frac{\tan \beta}{\sqrt{H_b/L_0}} \quad (1.16)$$

determines the breaker type [32], where β is the seabed slope and L_0 is the wave length in deep water. For $\xi_b < 0.4$ spilling breakers occur that are similar to regular waves at breaking limit, for $0.4 \leq \xi_b < 2.0$ plunging breakers occur, and for $\xi_b > 2.0$ surging breakers occur. Plunging breakers are the most problematic for wind turbines, as the overturning wave crest can lead to impulsive forces at impact that are more than one magnitude higher than typical wave forces from non-breaking waves.

Breaking waves and their loads have been studied for monopile foundations [33] and recently also for jackets [34, 35], but due to the instable, random nature of the breaking process (that involves air entrainment in the breaker front), there exists considerable uncertainty regarding the loads during wave breaking events.

1.2.8 Extreme waves

For engineering purposes it is important to understand the extreme wave conditions that can occur at a given site. The problem is often split into two tasks. First, an extreme seastate is determined that corresponds to a given return level, e.g. a “50-year” seastate with an annual exceedance probability of $1/50$. Then the highest wave in such storm conditions is determined, typically assuming a storm duration of 3 hours.

Let us consider the second problem first. The highest wave in a given time interval can be estimated statistically (see e.g. [36]), but simulation of such a wave with an appropriate theory (e.g. Stokes 5-th order) results in a regular wave that does not accurately predict the wind turbine response. An alternative is to simulate irregular waves and the turbine response during the full time interval of the storm, but this is computationally expensive. The state of the art is to generate the most probable extreme wave by aligning the wave frequency components (with zero phase difference) and suitably modifying the amplitudes. This embeds the desired extreme wave in a realistic irregular wave field that is convenient for response simulations. The approach is known as the NewWave theory⁴ [37].

Returning to the first problem, this is typically addressed by fitting an extreme value distribution to the available data (e.g. wave height timeseries) and extrapolating to the desired return level [38]. However, the seastate is in general not described by a single parameter, and one has to find a multivariate extreme value. These are not uniquely defined but rather result in a contour line (e.g. of the spectral parameters T_p versus H_s of suitably extreme seastates). The classical way to deal with this is to fit a parametric distribution to the data with specified statistical dependence, for which

⁴A similar approach can be used for efficiently simulating extreme wind events.

extreme quantiles can be obtained analytically. However, it is possible to estimate the dependence between seastate parameters directly from data using so-called copulas [39].

It should be remarked here that the actual design problem is often not determining the extreme environmental conditions, but rather determining the environmental conditions with the most extreme response (due to dynamic amplification these are typically not the same). This is a difficult problem, and only approximate solutions are known. The state of the art in determining an extreme seastate for a defined structural failure probability is the environmental contour method [40], an extension of the Inverse First Order Reliability Method (IFORM).

1.2.9 *Taifuns and hurricanes*

Extreme storms such as taifuns and hurricanes result in special environmental conditions that are not well characterized by standard approaches and for which special considerations should be made. For example, the wave field is more asymmetric; this effect can be modelled with a JONSWAP sea state spectrum by modifying the fetch parameter [41]. Of course also the wind loads need to be modified appropriately, for which some guidance exists [42]. An alternative is the use of climate simulation models to derive approximate environmental conditions during storm passage [43].

1.2.10 *Directional spreading*

In real sea conditions only multi-directional (short-crested) waves are found. The waves typically occur with a preferred direction, and the variability of the wave direction can be described with a statistical spreading distribution,

$$D(\theta; f) = \frac{S(f, \theta)}{S(f)} \quad (1.17)$$

where $S(f, \theta)$ is the full two-dimensional wave spectrum evaluated at frequency f and direction θ . The dependence on frequency is often neglected, and a number of models have been proposed for describing the observed wave directionality [44].

Probably the most widely used one is the $\cos^{2s} \theta$ model,

$$D(\theta) = \frac{\Gamma(s+1)}{\Gamma(s+\frac{1}{2})2\sqrt{\pi}} \cos^{2s} \left(\frac{\theta}{2} \right). \quad (1.18)$$

The parameter s is related to the directional width

$$\sigma_{\theta}^2 = \int_{-\pi}^{\pi} \left(2 \sin \left(\frac{\theta}{2} \right) \right)^2 D(\theta) d\theta \quad (1.19)$$

by $\sigma_{\theta} = \sqrt{\frac{2}{s+1}}$.

This directionality of waves was often neglected in the past, e.g. due to limitations of software and computational resources, and ocean waves are still mostly being modelled as long-crested (planar) waves for engineering purposes as of today. However, the two-dimensional nature of the directional spreading of waves around

the mean direction can lead to significant differences in wave loads, which is relevant for offshore wind turbines [45].

1.2.11 Currents

The presence of an ambient current U (e.g. due to tides or a storm surge) can change the amplitude, frequency and direction of waves. Current-wave interaction transfers energy between waves and currents, which needs to be accounted for in large-scale wave models. Two important additional effects are the shifting of frequencies and current-induced refraction. The former is similar to the familiar Doppler shift, so in a fixed frame of reference the absolute frequency is $\omega = \sigma + kU$, compared to the relative frequency σ (the frequency measured in the frame moving with the current) of the wave.

A second, higher-order effect is that a non-uniform ambient current induces a change in the wave direction. This is similar to the effect that a change in water depth has on the wave direction.

Finally, it is noteworthy that the water particles in a linear wave move not on closed orbits, i.e., a net transport of mass occurs. This so called Stokes drift is only one of the possible mechanisms by which waves induce currents. However, in engineering practice these later effects are typically not relevant.

Currents complicate the evaluation of wave loads. For fixed structures the traditional approach is to simply superpose the current velocities on the wave velocities and then use the Morison approach (see next Section), but experiments indicate that this is only an approximation of the actual wave loading.

1.3 Wave structure interaction

In Section 1.1 the concept of slender structures, not altering the surrounding wave field was introduced, as opposed to larger ones, yielding diffraction effects. For those larger ones, or structures with multiple bodies (i.e. column-stabilized FOWTs), the Boundary Element Method (BEM) solves the potential flow problem, introduced for linear waves in Section 1.2.2, including the body boundary conditions. The boundaries are discretized in the form of panels, and the correct boundary conditions are modelled with sources, sinks and dipoles, see [46, p. 102]. Analytic solutions exist for cylindrical shapes, but also for non-cylindrical shapes through conformal mapping techniques (so-called Lewis forms), see [17]. This method is usually used for floating structures, see Section 1.3.3. Slender structures can be modeled with semi-empirical Morison's equation, see Section 1.3.4, using the wave kinematics of Section 1.2.2

The regimes, in which the two assumptions hold are shown in Figure 1.2, using a nondimensional description of the characteristics of the wave forcing on a body. On the abscissa is the diffraction parameter ka , the product of the wavenumber k and the body radius $a = D/2$, which can be expressed with the wavelength λ as $ka = \pi D/\lambda$. The vertical axis is the Keulegan-Carpenter number, which can be expressed in two

ways, with the fluid velocity amplitude \hat{v} and the wave period T or with the fluid excursion amplitude \hat{x} , see [3, p. 12-16]

$$KC = \frac{\hat{v}T}{D} = 2\pi \frac{\hat{x}}{D}. \tag{1.20}$$

The wave breaking limit $H/\lambda = 1/7$ for deepwater waves is shown in Figure 1.2. It is independent of the body dimensions, see [3, p. 13-4]. Inertial loads (acceleration-dependent) are dominant for small KC number, whereas drag becomes more important for larger KC . In a given sea state a FOWT spar will therefore be more drag-dominated than a deepwater offshore structure of larger diameter. The latter will also be more likely to cause significant diffraction as ka increases with the diameter. This means that in this case a potential flow-solution or an additional diffraction correction model is necessary for Morison's equation (which neglects diffraction). In general, the diffraction effect is important for $ka > 0.5$, see [47, p. 174]. Both, potential flow theory for floating bodies in waves, as well as Morison's equation will be introduced in the following, together with an extension of the wave force models for the time-domain.

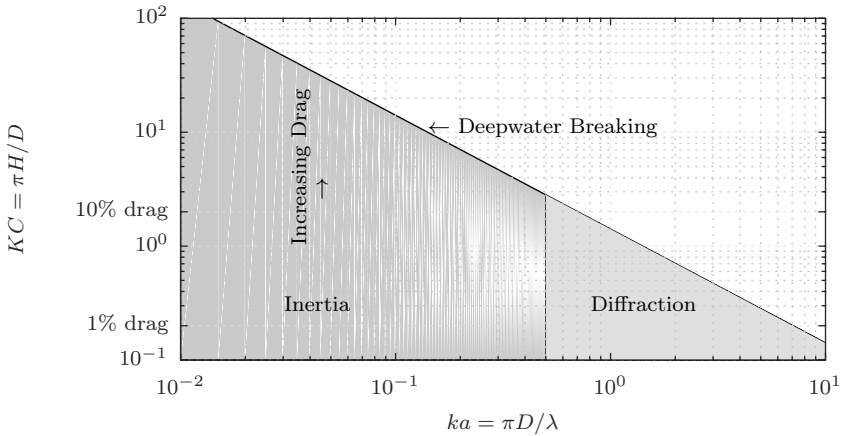


Figure 1.2 *Wave-induced force component domains. Taken from [24], originally from S.K. Chakrabarti.*

1.3.1 *Hydrostatics*

For FOWTs, the hydrostatic properties represent the most fundamental constraint for the structural design of floating offshore substructures. It determines the hydrostatic buoyancy (basically the ability to support the wind turbine mass without sinking), the stability and the restoring characteristics of the floater under static design loads. For example hydrostatics determine the static pitch inclination of the floater under maximum rotor thrust, which often is an important initial design driver. During the design process, the hydrostatic properties can be obtained using simple analytic

approximations. These are often called spreadsheet calculations and require inputs such as the center of gravity and the hull shape characteristics. The hull shape determines the submerged volume, the center of buoyancy (center of submerged volume) and the horizontal cross-sectional area (waterplane area). The restoring stiffness in vertical (heave) direction is given according to [17] by

$$C_{33} = \rho_w g A_{wp} \quad (1.21)$$

with the waterplane area A_{wp} in the xy -plane, the water density ρ_w and the gravity constant g . The hydrostatic restoring stiffness C_{55} in pitch-direction is clearly important due to the necessary reaction to the aerodynamic thrust force at hub height. It can be calculated with the second moment of the waterplane area

$$I_{22,wp} = \iint_{A_{wp}} x^2 dx dy \quad (1.22)$$

and remains with the submerged volume ∇ and the structural mass m as

$$C_{55} = \rho_w g I_{22,wp} + \rho_w g \nabla z_{cb} - mg z_{cm}. \quad (1.23)$$

The distance of the center of buoyancy z_{cb} and the center of gravity z_{cm} from Still Water Level (SWL), here positive in downward direction, is the main contributor to the restoring for spar-type platforms since the waterplane area is very small. For symmetric, free floating bodies $C_{44} = C_{55}$ holds and all other entries of the hydrostatic stiffness matrix $\mathbf{C} \in \mathbb{R}^{(6 \times 6)}$ are zero.

For floating substructures, the hydrostatic intact and damage stability needs to be assessed. Stability in this context refers to a measure of resistance to either capsizing or heeling. The analysis is typically performed by applying special software packages which, based on the discretized hull surface geometry, compute righting arm (GZ) curves for various loading and flooded conditions. For the analysis, the heeling moments by wind and other forces must be computed, and the righting lever must be compared to the heeling lever. The hydrostatic restoring forces and moment are traditionally computed using a linear hydrostatic approach, assuming the submerged structure is a rigid body (structural flexibility and deformations are ignored). The computation assumes that the hydrostatic restoring force and moment are due to infinitesimal changes of translational and rotational displacements. The change in hydrostatic forces and moments is represented using a stiffness matrix conventionally calculated at the initial static equilibrium position. In reality, hydrostatic restoring forces and moments are nonlinear (if measured relative to a fixed reference frame), for floating wind substructures particularly in roll and pitch. The hydrostatic nonlinearity can increase motion response amplitude and lead to capsizing. The influence of nonlinearity is most important for large displacements and couplings among heave, roll, and pitch — such large displacements are common for floating wind turbines. Moreover, external aerodynamic and hydrodynamic loads on the substructure and wind turbine are functions of the response and are directly influenced by the relative velocity and acceleration between these loads and the system components on which they act. Methods exist to analytically calculate the nonlinear hydrostatic restoring accurately for common geometrical shapes, and iterative

numerical methods can be applied for complex geometries to obtain the nonlinear restoring. Structural flexibility can also be accounted for by e.g. taking into account one or more deflection eigenmodes.

1.3.2 Fixed structures

The main boundary conditions for the hydrodynamic analysis are given by the wind, wave (including directionality and joint probabilities) and soil characteristics. Following the metocean and geotechnical analyses and considering the particular failure and operating modes of the wind turbine as well as symmetry aspects of the substructure, the load case table (LCT) setup is defined. The LCT outlines the conditions for every single load simulation to be run to determine the ultimate and fatigue loads for the design load cases defined in the selected standard. Typically the designs are performed according to standards such as IEC61400-3 or DNV-OS-J101, requiring natural frequency analysis (NFA), extreme event / ultimate limit state analysis (ULS), fatigue limit state analysis (FLS), serviceability limit state analysis (SLS), accidental limit state analysis (ALS) and, in case the structure contains slender members (jackets or semi-submersible floaters), vortex shedding analysis (VSA).

In terms of numerical methodologies and software, for the substructure design, as primary loads (external loads from aero- and hydrodynamics) and response (structural responses, load effects) analysis tools, flexible finite element beam-based or flexible multibody methods are used to perform static or dynamic (incl. spectral) analysis of spatial frames, truss structures and piping systems subjected to various kinds of loads (gravity, acceleration, transport, temperature, pressure, buoyancy, wave, current and wind). Finite shell element or volume element based approaches are typically used for analyses of details such as influences of welded attachments on the primary structure, complex plated structures such as the flange between the pile and the transition piece and to investigate pile buckling particularly near mudline and increased ovalization of the pile. The accurate representation of soil structure interaction is important for fixed-bottom structures, where typically a subgrade modulus method with non-linear and depth dependent load-deformation (p-y) characteristics of the soil springs is utilized. If sufficient information on soil properties and sophisticated constitutive models are available, more advanced FE based methods are also applicable, which reveal more physically realistic failure modes.

The modelling of fixed offshore wind substructures in terms of hydrodynamics relies mostly on approaches based on the Morison equation. While the assumption of hydrodynamically transparent structures is often not valid anymore for large diameter monopiles (> 10m), the Morison equation is still applicable if the empirical parameters are calibrated accordingly. Potential flow based radiation/diffraction theory is usually not applied for fixed structures. One reason for this is because these approaches cannot be used with higher order wave models, necessary to represent non-linear steep waves common in shallow water depths where fixed structures are located. Methods which are applied for larger diameter fixed structures are therefore based on the MacCamy and Fuchs approach that establishes an analytical closed form solution to the linear wave diffraction problem for free surface piercing cylindrical vertical structures. The theory originally was derived for Airy waves, but has

been extended also to second order waves.

While sophisticated load simulation tools exist for both offshore structures and wind turbines, the model choice depends often not only on the technological capabilities but on the availability of detailed model data. Due to the commercial project reality regarding confidentiality and distribution of responsibilities and associated risk, a number of alternative approaches are applied. These methods need to account for the practical limitations in industry, regardless of today's tool capabilities for performing coupled integrated loads analysis. This is considered a key difference to FOWT design, where, at least for the final detailed design, only a fully integrated simulation approach is considered to be viable to accurately determine the loads. Load calculation approaches common for fixed-bottom design can be distinguished in:

- Superimposed method, characterized by isolated aerodynamic (no waves) and hydrodynamic load simulation (no wind⁵) with simplified boundary conditions
- Sequentially integrated method, represented by iterative load simulations using compatible tools
- Holistic integrated approach using fully coupled models

1.3.3 Floating structures: Linear theory

The linear, first-order coefficients of the floating rigid body equation of motion can be solved with hydrodynamic panel codes with 3D surface meshes as boundary conditions. Usually the decoupled problems of radiation (or maneuvering) and diffraction (or seakeeping) are considered, see [2, Section 6.19]: The radiation problem is solved for still water with the floating body boundary oscillating at various frequencies. Its linear solution is the frequency-dependent radiation damping matrix $\mathbf{B}(\omega) \in \mathbb{R}^{(6 \times 6)}$ and the frequency-dependent added mass matrix $\mathbf{A}(\omega) \in \mathbb{R}^{(6 \times 6)}$. The diffraction problem is solved for a fixed floating body with waves of different frequencies (and directions) as boundary condition. The linear solution of the diffraction problem is the frequency-dependent wave excitation force coefficient $\mathbf{X}(\omega) \in \mathbb{R}^{(6 \times 1)}$, which gives, multiplied with the wave height amplitude spectrum A_ζ , the first-order force spectrum $\mathbf{A}_F^{(1)}$. All coefficients are lumped quantities, calculated with respect to the selected reference point. In the frequency-domain the equation of motion can be set up assuming a linear superposition of the radiation and diffraction problem, resulting in

$$-\omega^2 [\mathbf{M} + \mathbf{A}(\omega)] \boldsymbol{\xi} + j\omega \mathbf{B}(\omega) \boldsymbol{\xi} + \mathbf{C} \boldsymbol{\xi} = \mathbf{X}(\omega) A_\zeta(\omega) = \mathbf{A}_F^{(1)} \quad (1.24)$$

with the complex vector of differential generalized coordinates of the unconstrained body in all three directions and orientations $\boldsymbol{\xi} \in \mathbb{R}^{(6 \times 1)}$ as

$$\boldsymbol{\xi} = [x_p, y_p, z_p, \alpha_p, \beta_p, \gamma_p]^T, \quad (1.25)$$

see also [2]. With Eq. (1.24) the Response Amplitude Operator (RAO) (\mathbf{A}_ξ/A_ζ) can be calculated, the transfer function from the wave height ζ_0 to the rigid-body generalized coordinates $\boldsymbol{\xi}$.

⁵The effect of the interaction between rotor motion and wind field known as aerodynamic damping is then typically modelled with a linear viscous damper at tower top.

The two potential flow solutions of the coefficients of the left and the right-hand side of Eq. (1.24) are specifically useful: The matrices $\mathbf{A}(\omega)$ and $\mathbf{B}(\omega)$ represent the system properties, whereas $\mathbf{X}(\omega)$ represents the excitation force coefficient of the wave force spectrum $\mathbf{A}_F^{(1)}$, on the right-hand side of the Equation of Motion (EQM).

1.3.3.1 Frequency-to-time-domain transformation

For time-domain simulations of freely floating bodies Cummins [48] derived a valid frequency-to-time-domain conversion of the EQM (1.24). The linear stationary description in the frequency-domain needs to be extended to account for the transient motion of the floating body (which can arise from wind-induced motion, transmitted through nonlinear force models, including the controller). In terms of hydrodynamics such a transient motion yields pressure forces due to radiated waves by a motion impulse of the hull. The frequency-domain dynamics of the bulk of fluid particles surrounding the hull are given by

$$\mathbf{K}(j\omega) = \mathbf{B}(\omega) + j\omega[\mathbf{A}(\omega) - \mathbf{A}_\infty]. \quad (1.26)$$

The ‘‘retardation’’ function $\mathbf{K}(j\omega)$ is composed of a real part, the damping coefficient, and an imaginary part, which is the added-mass coefficient. The time-domain fluid impulse response function $\mathbf{K}(t)$ can be obtained according to Ogilvie [49], by transforming either the real part or the imaginary part of Eq. (1.26) to the time-domain as

$$\mathbf{K}(t) = \frac{2}{\pi} \int_0^\infty \mathbf{B}(\omega) \cos(\omega t) d\omega = -\frac{2}{\pi} \int_0^\infty \omega [\mathbf{A}(\omega) - \mathbf{A}_\infty] \sin(\omega t) d\omega. \quad (1.27)$$

Consequently, the retardation function $\mathbf{K}(j\omega)$ can be computed from the panel code results yielding the impulse response function $\mathbf{K}(t)$ after a suitable Fourier transformation.

The integral radiation pressure forces can now be written in the time-domain with an acceleration-dependent term with the constant coefficient \mathbf{A}_∞ and the convolution of the impulse response function $\mathbf{K}(t)$ with the body velocity $\dot{\boldsymbol{\xi}}$ according to Cummins, [48], as

$$\mathbf{F}_{rad}(t) = -\mathbf{A}_\infty \ddot{\boldsymbol{\xi}} - \int_0^t \mathbf{K}(t - \tau) \dot{\boldsymbol{\xi}} d\tau. \quad (1.28)$$

This is commonly implemented in state-of-the-art floating wind simulation tools such as FAST, see [50], and others. The resulting Cummins’ equation

$$(\mathbf{M} + \mathbf{A}_\infty) \ddot{\boldsymbol{\xi}} + \int_0^t \mathbf{K}(t - \tau) \dot{\boldsymbol{\xi}}(\tau) d\tau + \mathbf{C} \dot{\boldsymbol{\xi}} = \mathbf{F}_{wave}(t). \quad (1.29)$$

is the time-domain equation of motion of a rigid floating body. The calculation of the exciting forces $\mathbf{F}_{wave}(t)$ in Eq. (1.29) in the time-domain is usually done with an Inverse Discrete Fourier Transform (IDFT). An alternative approach is presented in the next section. The convolution integral of Eq. (1.29) brings some computational burden since a time history of platform velocities has to be stored and an integration over a number of past timesteps is necessary. The number of timesteps necessary has to be determined according to the hull shape.

1.3.3.2 Parametric models

Various approaches exist to develop unified state-space models that approximate (1.29). The objective of this is to obtain linearized hydrodynamic models, which can be more readily transformed into the time-domain. The term “parametric” here means a Linear Time-Invariant (LTI) model with a nonzero number of states (in the case of a state-space model), or poles (in the case of a linear transfer function). Using methods of system identification, a new LTI model is established that represents the best fit to the original model from the panel code, and which depends only on a few parameters/coefficients. A toolbox for identifying the state-space model for the forces of radiated waves from body motion has been developed in [51]. Based on this, a functionality has been added to the wind turbine simulator FAST, see [52].

An even simpler approach to avoid the convolution integral (1.29) is to approximate the frequency-dependent added mass $\mathbf{A}(\omega)$ through its value at representative frequencies. This “constant matrix” approach, reported in [53], was assessed for FOWTs in [24] with promising results.

Next to the radiation problem, also the wave force excitation coefficient $\mathbf{X}(\omega)$ can be approximated by a linear state-space model, as proposed by [54] and applied to FOWTs in [55]. The input to the parametric wave excitation model is simply the wave height as “measurable sensor” instead of the hydrodynamic forces, which are the simulation inputs in other models. These “disturbance models” are essential for vessel stabilization and disturbance rejection such as Dynamic Positioning (DP) control of offshore support vessels. For FOWTs, with complex excitations from wind and waves, such disturbance rejection methods are very promising, see [56] for model predictive control and [57] for feedforward control using look-ahead wind measurements.

1.3.3.3 Second-order slow-drift forces

The first-order force transfer function $\mathbf{X}(\omega)$ of Eq. (1.24) is a linear description of the wave forces as response to the wave spectrum. If a panel code representing the second-order potential, from the nonlinear component of Eq. (1.5), is used and integrated up to the free surface additional terms are added to the force-RAO, $\mathbf{X}(\omega)$, Eq. (1.24) see [46]. The purely quadratic terms of the wave height ζ are usually neglected in this quadratic correction to the linear BEM. But additionally to these, forces at the sum and difference of two wave frequencies result. These are products of first-order terms of the two wave frequencies. Various BEM solvers can compute the Quadratic Transfer Function (QTF), giving the wave forces from two linear wave components. The low-frequency force (at the difference frequency) may result in large amplitudes of motion of the floating body and consequently large loads on the mooring system. The sum and difference-frequency is equal to the so-called beat frequency of the two waves, a phenomenon which exists also in acoustics. The difference-frequency is the one of the bounded long waves, which result from the envelope of a wave group, see [3].

The second-order potential can be solved with pressure integration at the floating body, called the nearfield solution. Computationally more efficient is the calculation

of the farfield solution (based on the momentum equation). However, in this case the forces are only available in two directions.

The slowly-varying drift force can be calculated based on the QTF, denoted by $\mathbf{T}(\omega, \omega)$, which results from nonlinear panel codes. The force spectral density matrix in the frequency-domain was given by Pinkster, see [58] as

$$\mathbf{S}_{FF}^{(2)}(\mu) = 8 \int_0^\infty \mathbf{T}(\omega, \omega + \mu) S_{\zeta\zeta}(\omega) S_{\zeta\zeta}(\omega + \mu) \mathbf{T}(\omega, \omega + \mu)^{*T} d\omega, \quad (1.30)$$

where μ is the difference-frequency of the bichromatic wave, $\mu = \omega_i - \omega_j$ and $(\cdot)^{*T}$ denotes the complex conjugate transpose. To simplify Eq. (1.30) Newman proposed in [59] to calculate the force spectrum $\mathbf{S}_{FF}^{(2)}$ with the diagonal $\mathbf{T}(\omega_i, \omega_i)$, only, instead of the full QTF. This is reasonable because the QTF does usually not vary much with the difference-frequency, see [46, p. 157]. The force spectrum with Newman's approximation results as

$$\mathbf{S}_{FF}^{(2)}(\mu) = 8 \int_0^\infty \mathbf{T}(\delta, \delta) S_{\zeta\zeta}(\omega) S_{\zeta\zeta}(\omega + \mu) \mathbf{T}(\delta, \delta)^* d\omega. \quad (1.31)$$

with $\delta = \omega + \mu/2$. In the time-domain, the forces result according to [59] from a double IDFT as

$$\mathbf{F}_{wave}^{(2)}(t) = \sum_i \sum_j A_\zeta(\omega_i) A_\zeta(\omega_j)^* \mathbf{T}(\omega_i, \omega_i) \cos[(\omega_i - \omega_j)t + \varphi_{\zeta,i} - \varphi_{\zeta,j}]. \quad (1.32)$$

Newman explains in [59] that the double summation over ω_i and ω_j of Eq. (1.32) can be written as the square of a single sum of suitably chosen frequencies of the arguments. In this case the time series result (formulation as in [60]) as

$$\mathbf{F}_{wave}^{(2)}(t) = \boldsymbol{\theta}^2 \Big|_{T(\omega_i, \omega_i) > 0} - \boldsymbol{\theta}^2 \Big|_{T(\omega_i, \omega_i) < 0} \quad \text{with} \quad (1.33)$$

$$\boldsymbol{\theta} = \sum_i |A_\zeta(\omega_i)| \sqrt{2|T(\omega_i, \omega_i)|} \cos(\omega_i t + \varphi_{\zeta,i}),$$

where $|A_\zeta(\omega_i)|$ is the wave amplitude magnitude at ω_i , calculated from the Power Spectral Density (PSD) numerically and $\varphi_{\zeta,i}$ is the corresponding phase angle. Note that the phase convention is here such that $\varphi = 0$ on the positive real axis. Although this formulation is computationally very efficient, it has the drawback that it contains unphysical high frequencies, which need to be filtered. An improved formulation was proposed by [61] with the product of two sums as

$$\mathbf{F}_{wave}^{(2)}(t) = \text{Re} \left(\left[\sum_i |A_\zeta(\omega_i)| \text{sgn}(T(\omega_i, \omega_i)) \sqrt{T(\omega_i, \omega_i)} \exp(i(\omega_i t - \varphi_{\zeta,i})) \right] \cdot \left[\sum_j |A_\zeta(\omega_j)| \sqrt{T(\omega_j, \omega_j)} \exp(i(-\omega_j t + \varphi_{\zeta,i})) \right] \right). \quad (1.34)$$

In Figure 1.3 the different formulations for the slowly varying drift force (Eq. (1.31)–(1.34)) are compared. Comparing the wave spectrum $S_{\zeta\zeta}(\omega)$ on top with the drift

force spectra $\mathbf{S}_{FF}^{(2)}(\omega)$ it can be seen that the drift forces introduce energy below the wave frequencies. The mean drift coefficients, calculated with the nearfield solution (direct pressure integration) are shown in surge-direction in the second plot. Below are the force spectra and the corresponding time series. The direct frequency-domain calculation, Eq. (1.31), gives the largest response magnitude. The second largest response magnitude results from the double sum approach, Eq. (1.32). Comparing the original Newman formulation, Eq. (1.33) with the improved formulation by Standing, Eq. (1.34), the response magnitude is the same at the (low) difference-frequency, only at frequencies above the wave spectrum the original Newman formulation shows another peak. These are the unphysical frequencies, which need to be filtered.

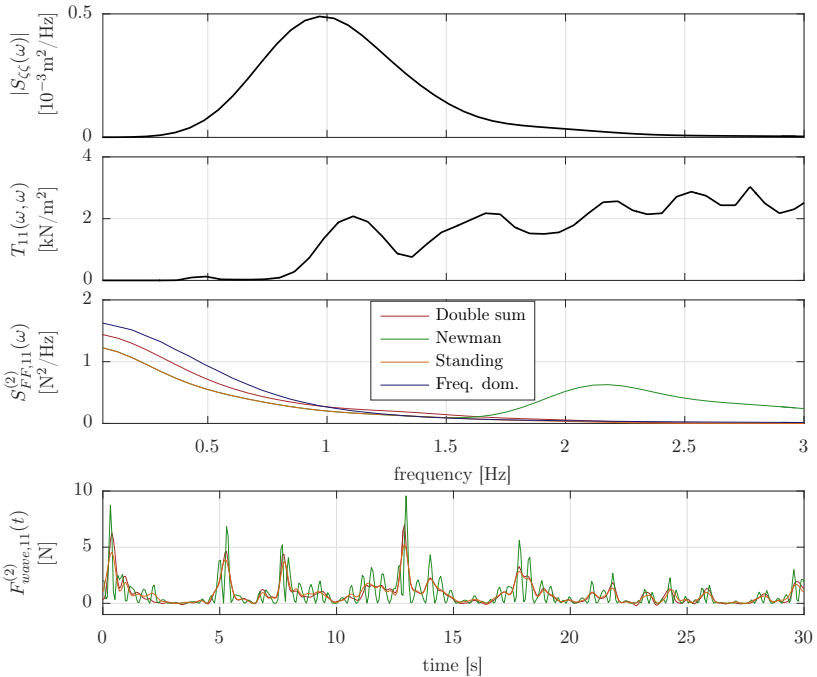


Figure 1.3 Wave spectrum (top), mean drift coefficients $T_{11}(\omega, \omega)$, surge slow-drift force spectrum $S_{FF,11}^{(2)}(\omega)$ and time series $F_{11}^{(2)}(t)$ with frequency-domain calculation (Eq. (1.31)), double IDFT (Eq. (1.32)), original Newman approximation (Eq. (1.33)) and Standing et al.'s formulation (Eq. (1.34)), from [24].

The formulation, implemented in the widely used HydroDyn model, see [50] and [60] of FAST [62] is the one according to Standing et al., Eq. (1.34). For the linearized frequency-domain model the spectral densities $\mathbf{S}_{FF}^{(2)}(\omega)$ are computed through a Discrete Fourier Transform (DFT) of the force time series of Eq. (1.34) in order to ensure equal difference-frequency excitation for both models.

1.3.4 Morison's equation

In recent simulation studies for FOWTs, Morison's equation has always been considered as an alternative option to the panel code method with Cummins' equation (as described in more detail later). Originally, Morison's equation was developed to model the ocean wave forces on slender piles fixed at the seabed, see [63]. It models the horizontal force $\Delta \mathbf{f}$ in the normal directions k of the body surface on a discrete "strip" i , which is a cylindrical section with diameter D and length Δl . The input to the force model are the undisturbed fluid accelerations a_{ik} and the velocities v_{ik} . Here, the Morison forces in the two horizontal directions are defined always in the inertial frame as

$$\frac{\Delta F_{ik}}{\Delta l} = k_M a_{ik} + k_D v_{ik} |v_{ik}| \quad (1.35)$$

with

$$k_D = \frac{1}{2} \rho C_D D \quad \text{and} \quad k_M = C_M \rho \pi \frac{D^2}{4}. \quad (1.36)$$

The inertia coefficient C_M results from the added mass coefficient C_A as $C_M = 1 + C_A$, giving the Froude-Krylov wave forces, represented by \mathbf{F}_{wave} in Eq. (1.29), as well as the added-mass forces. It can be shown that Morison's equation equals the panel code results for low frequencies with $C_A = 1$, see [47]. As with the coefficient for the drag C_D , contributing to the velocity-dependent force, also the added-mass coefficient has to be determined from experiments, high-fidelity CFD calculations or, for simple geometries from the literature, e.g. [64].

For floating platforms Morison's formulation was extended using the relative motion of the water particles $v_{w,ik}$ with respect to the floating body velocity $v_{b,ik}$ and their derivatives $\dot{v}_{w,ik}$ and $\dot{v}_{b,ik}$ such that Eq. (1.35) uses the coefficients

$$v_{ik} = v_{w,ik} - v_{b,ik} \quad \text{and} \quad a_{ik} = \dot{v}_{w,ik} - \dot{v}_{b,ik}. \quad (1.37)$$

Here, the coefficient k_M can also be split to obtain one coefficient for the fluid acceleration $\dot{v}_{w,i}$ and another one for the body acceleration $\dot{v}_{b,i}$, where the first models the Froude-Krylov and the latter the radiation added mass, c.f. Eq. (1.29), see [65]. The fluid kinematics are usually calculated assuming "hydrodynamically transparent" structures, meaning that the body does not alter the fluid motion and diffraction effects are negligible, as in the case of spar-type platforms ($ka < 0.5$). With Morison's equation the added mass force (first part of Eq. (1.35)) is independent of the frequency. This simplification is valid for structures with little radiation forces, as is usually the case for slender structures. Using linear wave theory the velocity $v_{w,ik}$ and acceleration $\dot{v}_{w,ik}$ can be calculated assuming a sinusoidal boundary condition at the free surface, see [3].

In summary, Morison's equation offers several practical advantages: Firstly, the pre-computation of the hydrodynamic coefficients $\mathbf{A}(\omega)$, $\mathbf{B}(\omega)$ and $\mathbf{X}(\omega)$ of Eq. (1.29) with a panel code can be avoided. Secondly, the distributed forces over the body surface can be obtained in a straightforward manner, as opposed to the panel code coefficients, which represent the integral forces over the wetted surface. This has the advantage that a continuum mechanics approach can be selected in or-

der to calculate the deformation and the structural stresses of the floating platform. This is only possible with Cummins' equation through a post-processing. The third advantage is a simple representation of the quadratic drag force with coefficients available in the literature for simple shapes. The Morison drag coefficients are usually defined such that they cover effects from flow separation and vortex shedding, which cannot be calculated with potential flow theory and is therefore not part of the radiation damping matrix $\mathbf{B}(\omega)$. This is due to the fact that linear potential flow does not include any dissipation model. A result of this assumption is d'Alembert's paradox stating that the wave particle velocity does not yield a force on a floating body. With potential flow the only force in the wave propagation direction is the acceleration-dependent Froude-Krylov force. Consequently, the viscous drag introduces the dissipative forces neglected by potential flow.

A common approach for modeling first-order wave forces on FOWT platforms is to combine the advantages of Cummins' equation with Morison's equation: 3D panel codes are flexible with respect to the hull shape geometry as no restriction on, e.g., the column diameter-to-wavelength ratio D/λ exists, as discussed with Figure 1.2. It is therefore straightforward to model e.g. barges or semi-submersibles with Cummins' equation. Morison's equation, on the other hand, includes the quadratic drag model. Therefore, the drag force component of Eq. (1.35) is often added to Cummins' equation (1.29), see e.g. [66]. As a consequence, third-order excitations become present in the time series of the response due to the velocity component, see last term of Eq. (1.35). For semi-submersibles a Morison drag term to model the vertical drag force from the horizontal plates (heave plates, damping plates) at the lower ends of the vertical columns needs to be added to complete the force calculation.

The transfer functions for the Froude-Krylov part are shown in Figure 1.4, without the velocity-dependent part, in order to compare them to the panel code results. The added mass coefficients were chosen such that the integral added mass from the panel code equals the added mass from Morison's equation. It can be seen that there is a fairly good agreement for low frequencies. In the introduction a limit of $ka = 0.5$ was given, above which diffraction becomes important, see Figure 1.2. The diffraction limit is here 0.997 Hz for $ka = 0.5$. Beyond this frequency the agreement is poor, especially in surge-direction. The wiggles result from the dependence of the kinematics on the longitudinal position and represent the interference of the wave length with the floater members, see Section 1.2.4.

1.3.5 Identification from model tests

Several methods to identify both Morison coefficients, added mass and viscous drag, are proposed in [3, p. 12-9] and [2]. Many of these methods, however, are aimed at reducing the computational effort, as full system simulations were not affordable in the past. Recently, methods have been proposed to tune the drag coefficients by running nonlinear simulations in order to identify the best fit of the response. The added mass is usually obtained from BEM models and not identified from model tests.

The question of how to upscale the viscous drag to prototype scale is still subject of current research. Here, CFD methods can be a solution to obtain the viscous

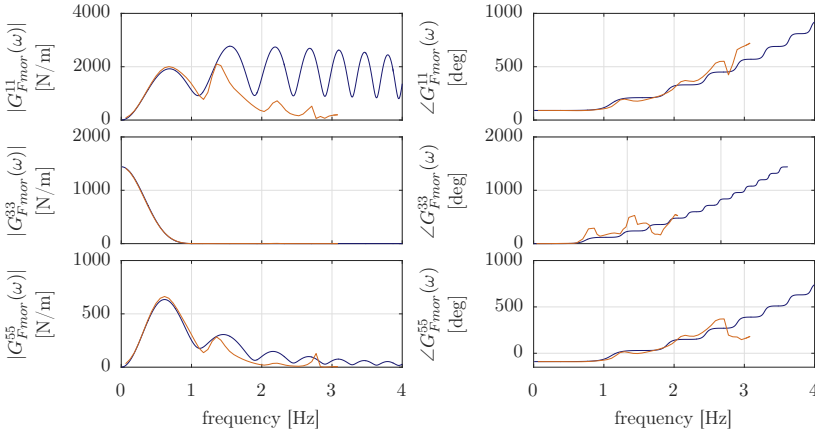


Figure 1.4 *Morison excitation transfer functions $\mathbf{G}_{Fmor}(\omega)$ for Froude-Krylov component only (blue) compared to panel code transfer functions $\mathbf{X}(\omega)$ (orange), from [24].*

drag coefficients for the different members of the hull in both steady flow and in oscillatory flow conditions. Drag calculation with combined structural and wave motion to obtain the wave drift damping might be necessary for certain FOWT types.

For floating wind substructures, model tests of the coupled system are often performed to not only calibrate viscous coefficients, but also to serve as a proof of concept and to validate coupled analysis results. Here challenges exist regarding the scaling of aerodynamic and hydrodynamic forces, which are governed by different dimensionless numbers. The Froude and Reynolds number in practise (in theory, the fluid density may be changed) cannot be scaled simultaneously. Therefore a number of approaches have been developed to overcome this problem. The two most widely used methods are either the Froude-scaling of the aerodynamic rotor thrust curve by changing the rotor geometry of the scaled physical wind turbine model in the wind-wave tank, or using software-in-the-loop approaches to compute the scaled thrust force from the rotor in realtime. Both approaches have their specific limitations and advantages, see [67] for a description and comparison of currently used methods.

1.3.6 *Hydro-elasticity*

Coupled FOWT models do usually assume that the floating platform is rigid. For the calculation of the structural stresses, however, it is necessary to account for the structural elasticity. So far, this is mostly done through de-coupled Finite Element (FE)-models. Recently, approaches have been presented to model the structural elasticity in coupled models. In this case, Cummins equation, Eq. (1.29) cannot use the integrated coefficients for the entire floater, but the distributed ones. Such an extension has been presented in [68] and [69], taking also the hydro-elastic interactions into account.

1.3.7 Wave overtopping and green water

A green water event occurs when an incoming wave exceeds the freeboard and water then runs on deck structures. This introduces additional loads and affects the dynamics and stability of the structure, which is especially relevant for floaters.

As important as it is, such events are typically analyzed with fully featured CFD simulations, as there is little guidance for evaluating green water events in a simplified way. Some recommendations have been given by Buchner [70], including possible mitigation measures (e.g. sloping decks). However, the main conclusion is that increasing the freeboard should be the preferred option.

1.3.8 Mooring System Interaction

Mooring system models combine structural mechanics for the representation of the mooring line itself with hydrodynamics for the computation of the external fluid forces and contact mechanics for the forces from line-seabed interaction. In general the marine environment continually disturbs each part of the mooring line by perturbation from surface waves, surface and subsurface currents, subsurface turbulence, and internal waves. The line responds to these disturbances with drift motions and translational and rotational oscillations along with structural deformations. In addition gravitational forces from the weight of the line in water are constantly forcing the line to assume a catenary shape. For lines with parts resting on the seabed, the line-seabed interaction in terms of friction forces on the line and damping must be considered as well, a problem where a wide variety of models exist. The resulting motion of the line in turn gives rise to motion of the platform, i.e. both systems are in general coupled, except for special built-in fairlead design features aiming to decouple the systems. Numerical mooring system models can generally be divided into two main categories: quasi-static and dynamic modelling approaches. For each of the two categories, different modelling methods exist as well as different implementations in integrated aero-servo-hydro-elastic models.

1.3.8.1 Quasi-static Models

Quasi-static models are characterized by the fact that at each instance in time the mooring system is in equilibrium, i.e. the model is time-invariant and for each displacement of the floater a unique restoring force can be computed, regardless of the history of the previous motions. This implies that no transient dynamic effects are considered, such as acceleration-dependent forces from inertia, viscous hydrodynamic drag forces, forces arising from bending, torsion and internal damping. The quasi-static models can be categorized into three main approaches:

- Linearized stiffness

The representation of the complete mooring system by a linear 6x6 stiffness matrix is the most simple approach to model a mooring system. It is only valid for small displacements around the reference (mean) displacement for which the linear stiffness matrix has been derived. Typical application of this approach is in early concept studies, or when a linear model is required.

- Look-up table

A nonlinear force-displacement relationship can be derived from either quasi-static or dynamic models (averaged) and then stored as a discretized 3D-lookup-table, where the restoring force is tabulated for each position of the floater in 3D-space. Using interpolation, the restoring force at any arbitrary position of the floater can be derived for each individual mooring line. The approach is able to capture the averaged non-linear restoring characteristics, but is also time-invariant.

- Analytical solution

Models based on analytical solutions of the implicit nonlinear catenary equations are the most common quasi-static modelling methodology.

As the analytical solution is the most common quasi-static solution, and also the underlying equations provide some insight into the parameters influencing the restoring force, a brief summary of the solution for a quasi-static line is provided, based on [71]. Further descriptions for floating wind mooring system models are found in [72]. Given a set of line properties, the line geometry can be expressed as a function of the forces exerted at the end of the line:

$$\begin{aligned}
 x(s) &= \frac{H}{\omega} \left\{ \ln \left[\frac{V_a + \omega s}{H} + \sqrt{1 + \left(\frac{V_a + \omega s}{H} \right)^2} \right] \right. \\
 &\quad \left. - \ln \left[\frac{V_a}{H} + \sqrt{1 + \left(\frac{V_a}{H} \right)^2} \right] \right\} + \frac{Hs}{EA} z(s) \\
 &= \frac{H}{\omega} \left[\sqrt{1 + \left(\frac{V_a + \omega s}{H} \right)^2} - \sqrt{1 + \left(\frac{V_a}{H} \right)^2} \right] + \frac{1}{EA} \left(V_a s + \frac{\omega s^2}{2} \right)
 \end{aligned} \tag{1.38}$$

where:

$$\omega = gA(\rho_{\text{cable}} - \rho) \tag{1.39}$$

and x and z are coordinate axes in the local (element) frame. The following substitution can be made for V_a in the above equations:

$$H_a = H \tag{1.40}$$

$$V_a = V - \omega L \tag{1.41}$$

which demonstrates that the decrease in the vertical anchor force component is proportional to the mass of the suspended line.

The equation (1.38) for $x(s)$ and $z(s)$ describes the catenary profile, provided all entries on the right side of the equations are known. In numerical tools, the horizontal and vertical force terms H and V are calculated, as the known quantities

typically are the fairlead position variables l and h . The forces H and V can be computed by numerically solving the following two implicit equations:

$$l = \frac{H}{\omega} \left[\ln \left(\frac{V}{H} + \sqrt{1 + \left(\frac{V}{H} \right)^2} \right) - \ln \left(\frac{V - \omega L}{H} + \sqrt{1 + \left(\frac{V - \omega L}{H} \right)^2} \right) \right] + \frac{HL}{EA} \quad (1.42)$$

$$h = \frac{H}{\omega} \left[\sqrt{1 + \left(\frac{V}{H} \right)^2} - \sqrt{1 + \left(\frac{V - \omega L}{H} \right)^2} \right] + \frac{1}{EA} \left(VL - \frac{\omega L^2}{2} \right) \quad (1.43)$$

The solution for the line in contact with a bottom boundary is found by continuing $x(s)$ and $z(s)$ beyond the seabed touch-down point $s = L_B$. Integration constants are added to ensure continuity of boundary conditions between equations.

$$x(s) = \begin{cases} s & \text{if } 0 \leq s \leq x_0 \\ s + \frac{C_B \omega}{2EA} [s^2 - 2x_0 s + x_0 \lambda] & \text{if } x_0 < s \leq L_B \\ L_B + \frac{H}{\omega} \ln \left[\frac{\omega(s-L_B)}{H} + \sqrt{1 + \left(\frac{\omega(s-L_B)}{H} \right)^2} \right] + \frac{Hs}{EA} + \frac{C_B \omega}{2EA} [x_0 \lambda - L_B^2] & \text{if } L_B < s \leq L \end{cases} \quad (1.44)$$

where λ is:

$$\lambda = \begin{cases} L_B - \frac{H}{C_B \omega} & \text{if } x_0 > 0 \\ 0 & \text{otherwise} \end{cases} \quad (1.45)$$

Between the range $0 \leq s \leq L_B$, the vertical height is zero since the line is resting on the seabed and forces can only occur parallel to the horizontal plane. This produces:

$$z(s) = \begin{cases} 0 & \text{if } 0 \leq s \leq L_B \\ \frac{H}{\omega} \left[\sqrt{1 + \left(\frac{\omega(s-L_B)}{H} \right)^2} - 1 \right] + \frac{\omega(s-L_B)^2}{2EA} & \text{if } L_B < s \leq L \end{cases} \quad (1.46)$$

The equations above establish the mooring line profile as a function of s . Ideally, a closed-form solution for l and h is sought to permit simultaneous solution for H and V . This is obtained by substituting $s = L$, resulting in:

$$l = L_B + \left(\frac{H}{\omega} \right) \ln \left[\frac{V}{H} + \sqrt{1 + \left(\frac{V}{H} \right)^2} \right] + \frac{HL}{EA} + \frac{C_B \omega}{2EA} [x_0 \lambda - L_B^2] \quad (1.47)$$

$$h = \frac{H}{\omega} \left[\sqrt{1 + \left(\frac{V}{H} \right)^2} - 1 \right] + \frac{V^2}{2EA\omega} \quad (1.48)$$

The tension in the line is a function of s along the line:

$$T_e(s) = \begin{cases} \max(H + C_B \omega(s - L_B), 0) & \text{if } 0 \leq s \leq L_B \\ \sqrt{H^2 + [\omega(s - L_B)]^2} & \text{if } L_B < s \leq L \end{cases} \quad (1.49)$$

Multi-segmented lines can also be modelled in a quasi-static manner by an extension of the singleline theory, where several singlelines define a multisegmented mooring line, see [71]. Here the challenge exists that a singleline solution is given in a two-dimensional domain, and a complete multisegmented line should be modeled as a system in a three-dimensional coordinate frame. This is achieved by coordinate transformations of the single line quantities to extend the theory to a three-dimensional representation. The unknowns for each line are solved in the local 2D frame and static equilibrium is ensured by solving for line properties that result in zero sum forces on the nodes in the 3D frame. This process requires two distinct systems of equations to be simultaneously solved to achieve the static cable configuration. The first set of equations are the force balance equations in three directions for each node, and the second set are the two catenary equations. More details are provided by Masciola. This problem requires an iterative solution process and convergence may depend on the numerical parameters of the chosen iterative solver.

1.3.8.2 Dynamic Models

The quasi-static methods described above do not account for mooring line dynamic effects, such as line inertia, the drag of the line through fluid, vortex shedding, structural damping effects, as well as contact and friction with the seabed. The dynamic effects are most important for an accurate prediction of the loads within the mooring line itself, as well as at the anchor and top connector. The loss of accuracy for loads in the wind turbine by applying a quasi-static mooring model in favour of a dynamic model is usually minor, because the global restoring forces from the mooring system are well predicted also by quasi-static models. Also the mooring system configuration influences the relevance of dynamic models. For example for systems where the total mass of the lines in the water column is small and the floater motions are limited, even though the drag force of the lines through the fluid still might be significant, dynamics can likely be neglected. When dynamic effects are important, a number of simulation approaches have been proposed for dynamic, non-linear mooring system models. The structural mechanical representations used by dynamic models are:

- **Lumped mass**
Usually lumped mass models apply an equivalent lumped mass approach, where the line is discretized into point masses connected by spring-damper elements.
- **Rigid or flexible finite segment**
In a finite segment approach (also lumped parameter), the line is discretized into several rigid or flexible bodies connected by massless spring-damper elements.
- **Finite element approaches**
Finite element approaches discretize the line usually into beams or volume elements connected via massless 6-DOF joints.

- Assumed modes

This approach uses methods using either monomials or shape functions from modal analysis to represent the line dynamics. The approach is rarely applied in offshore wind applications.

The hydrodynamic forces on the mooring line are typically represented by Morison-based approaches, described in another section in this chapter. Morison equation is well applicable as the mooring line can be considered as hydrodynamically transparent.

Even with dynamic mooring line models it is difficult to capture vortex induced vibrations (VIV). This effect is caused by steady currents or by the velocities associated with long-period waves and the resulting vortices shed behind the cylindrical line due to the viscous deceleration of the flow in the boundary layer. The effect refers to the dynamic loading that occurs as a result of fluctuations in pressure due to the motion of vortices being shed asymmetrically in the wake of a body. VIV in principle can excite the mooring line or tendon into vibrations, causing additional fatigue damage. Mooring systems can be analysed for VIV by advanced CFD methods or scaled wave tank tests. However, for typical mooring system configurations in floating wind, VIV are no issue and such advanced CFD or wave tank test methods are usually only applied for ultradeep Oil and Gas mooring systems.

To model the interaction of the line and the seabed, a contact model is required. Seabed interaction can be separated into two scenarios: tangential friction between seabed and line, if the line is resting on the seabed and pulled in tangential direction; and lifting and grounding interactions, which is a transient effect and occurs in the proximity of the touch down point (TDP) region, when the line settles on the seabed. In mooring system modes representing the whole mooring system, both scenarios are usually treated with the simplified numerical methods. The most simple approach is to apply a unilateral spring-damper contact force in normal direction (global z-direction) to the seafloor. This represents the elastic properties of the seabed, so that a line segment establishing contact with the seabed behaves realistically, and e.g. does not bounce off or dig in too much. The resulting normal force is output for usage in the lateral friction computation. This approach of representing the soil as a bed of linear springs is also used in the O&G industry to model the line-seabed interaction. For the derivation of the linear spring stiffness and damping, geotechnics offers various approaches with varying complexity, such as the subgrade reaction method, representing the most simple approach in geotechnics, or methods using the capacity bearing curve for a strip footing in drained soil to derive the soil stiffness as a secant stiffness to a nominal embedment. To represent the friction force in tangential direction along the seabed surface acting on line segments in contact with the seabed, a Coulombic non-linear friction force is applied using the normal force.

The computational speed of the dynamic mooring system models is sensitive regarding both physical model parameters and numerical solver properties. Segmented mooring line models represent serial kinematic chains, which because of the inherent

relationship of each segment to another (i.e. the anchor segment by induction carries all other segments) may lead to ill-conditioned mass or inertia matrices of the system and ultimately a long simulation time. Despite its relative simplicity in the equations, the contact modelling often has a significant contribution to the computational time. This negative effect is particularly imminent, if a line segment is frequently in and out of contact with the seabed so that a friction force on the line bodies is either applied or not applied; i.e. the right hand side of the equations of motion is frequently changing abruptly.

More information on dynamic mooring line models for floating wind applications can be found in [73].

1.3.8.3 Other mooring line modelling aspects

Apart from the above mentioned quasi-static or dynamic mooring models, further challenges exist:

- For steel chain mooring lines, individual chain links and their interaction, including effects such as out-of-plane bending or wear and tear, as well as pitting and other local effects influencing fatigue lifetime, are not included in today's models.
- For synthetic mooring lines, the non-linear stiffness, thermal and structural effects of the individual fibres and strands interaction, and material degradation are not considered in mooring design codes.
- Marine growth and corrosion are only represented by simplified approaches, such as increases of diameter and drag coefficients.
- Line and anchor soil interaction is usually considered by simplified models, at least for global analyses.
- Effects like erosion around the line, sinking, suction, lay angle of the line, or other effects affecting the contact model properties are neglected. Soil hysteresis, while generally possible to be represented with the selected model, is also neglected.

1.3.9 Representation of viscous Effects

Ideally, simulations models should be able to compute viscous (drag) forces on structures from first principles. However, due to the complicated flow patterns that occur under periodic motions, when turbulent flow features interact with themselves, such effects are challenging to represent accurately in models. Whereas this has been somewhat solved for slender-elements with the Morison approach, the issue is of particular relevance for the design of motion suppressing devices such as heave plates, commonly used with FOWTs. Typically model tests are needed to determine accurate damping coefficients, but some success has been achieved recently with both RANS and LES simulation approaches [74, 75].

1.3.10 Vortex induced vibrations

When a fluid moves around a structure, both drag and lift forces are induced. The drag force has been considered previously (Section 1.3.4). The lift force depends on the flow characteristics and the type of structure. For a structure in steady flow (e.g. due to a current), vortices are being shed from the boundary layer with a characteristic frequency given in terms of the Strouhal number S ,

$$f = \frac{SU}{D}, \quad (1.50)$$

and with periodically varying lift coefficient. For a cylinder, $S \approx 0.2$. Severe vibrations can occur when the shedding frequency is similar to the (first) eigenfrequency of the structure. More information on this and related flow-induced vibration phenomena can be found in the monography by Blevins [76].

In waves, the lift forces reverse every half cycle, and it is the KC number that determines whether vortex shedding occurs. For a cylindrical structure, vortex shedding occurs for $KC > 3$. For $KC > 5$ the vortices are being shed asymmetrically, and the cylinder experiences a periodically varying lift force. This force has frequencies corresponding to the wave frequency and its multiples. There does not currently exist an analytical model of the lift force under such conditions, but a model based on some simplifying assumptions is available (see e.g. [77]) that predicts forces of the form

$$f(t) \propto AC_L U^2 \sin^2 \omega t \cos(\alpha(1 - \cos \omega t) + \psi). \quad (1.51)$$

Here ω is the wave frequency, and $\alpha = KC \cdot S$ modifies the force variations.

Vortex induced vibrations (VIV) could be important for mooring chains and cables, as well as for jacket members. Due to the complex geometry at jacket joints, evaluation of the risk and loading from VIV has to be performed with CFD.

1.3.11 Ringing

Ringling of offshore structures is the phenomenon that steep, nonlinear waves can introduce additional higher-order harmonic loads that are not described by the Morison formula. For cylindrical structures these loads are related to a secondary load cycle that appears for steep waves shortly after the main load peak [78], and can be reproduced experimentally. Rainey derived second-order accurate corrections to the Morison approach that predict an additional ‘‘oblique slamming’’ load component at three times the wave frequency,

$$F = -\frac{1}{8} \pi \rho g k^2 D^2 a^3 \cos 3\omega t, \quad (1.52)$$

in terms of wave amplitude a , structure diameter D and wavenumber k .

The well-known FNV theory performs an analysis of the third order wave potential resulting in load components at two and three times the wave frequency [1],

$$F = \pi \rho g k D^2 a^2 \cos 2\omega t - \pi \rho g k^2 D^2 a^3 \cos 3\omega t. \quad (1.53)$$

However, the FNV theory is inaccurate for moderately large diameters and does not predict the secondary load cycle. Nevertheless, it is able to successfully pre-

dict higher-order resonant response in offshore structures. Such higher-order nonlinear loads occur at frequency ranges that are relevant for offshore wind turbines on monopiles and their fatigue analysis.

Also for floaters these loads play an important role. Especially the TLP is susceptible here due to its low eigenperiod [79]. For an accurate response analysis, Bachynski & Moan recommend using the second-order QTF together with third-order FNV loading, while considering only sum-frequency wave components [80].

1.3.12 Wave-soil interaction / Erosion

Geotechnical issues are more generally discussed in a separate chapter, but we mention here two important issues that are specific to offshore foundations.

In areas with erodible seabeds (e.g. consisting of sand), the seabed is a dynamic environment that continuously changes due to the effect of waves and currents. This can lead to complex sand wave patterns moving in time [81]. Additionally, the presence of a structure changes the flow around it, which leads to loss of material around it. This so-called scour can lead to loss of foundation stiffness and stability, and needs to be assessed during the design of offshore wind turbines, or mitigated using available scour protection technology [82, 83]. The largest scour development typically occurs during periods with very large waves, such as storm events, and the process can be simulated with the CFD approach.

As wind turbine foundations are subject to cyclic loads from waves and the rotor, the cyclic behavior of soils supporting the turbines is important. Cycling loading generates excess pore pressures and contributes to the development of shear strains in the soil, thereby leading to loss of stiffness and, in the extreme case, to a “liquefaction” of soils. Assessing the stiffness degradation is challenging and ultimately limited due to uncertainties about actual soil properties [84]. The effect can be modelled with finite element soil simulations for individual cycles, but a major computational challenge is to predict the long-term stiffness degradation for a large number of cycles.

1.3.13 Ice-structure interaction

Sea ice can be an important loading condition in some areas. The assessment of sea ice conditions is complicated by the fact that ice-structure interaction is not a one-way coupling: the ice gets compacted and eventually fails when the wind turbine moves into the ice (or vice versa). Ice failure by crushing results in loss of ice load, which results in acceleration of the turbine, possibly triggering another crushing event. This mechanism has been found to result in coupled vibrations at the natural frequency of the turbine for a large range of ice velocities in the so-called frequency-locking regime, resulting in considerable fatigue damage.

However, due to the complexity of the ice behavior, there currently does not exist an accurate ice-structure interaction model, and only highly simplified ice load models are in use. For example, ISO19906 recommends the use of a sawtooth ice load forcing function that is periodic with the natural period of the structure [85]. Some progress has been made recently with a stochastic piecewise-smooth model

that is able to reproduce the three main ice-structure interaction regimes [86], by modeling non-simultaneous ice failures (as suggested by e.g. Ashby [87]). The insight from this model has resulted in a spreadsheet procedure for preliminary ice risk analysis [88]. Apart from this, the main alternative seems to perform expensive CFD calculations of ice-structure interaction, but this has not been fully explored yet.

1.4 Limitations and current developments

Many of the described modeling approaches in this chapter involve assumptions, which limit the validity of the models. Here, the increasing computational power can help to realize computationally more demanding models of higher fidelity. Especially, cases with large nonlinear sea states and motion responses cannot be covered by today's engineering models. A simulation of stochastic load cases for fatigue assessment in the time-domain with high-fidelity models such as CFD, however, is today not yet realizable. On the other side, a multidisciplinary design optimization will require a good trade-off of the computational cost of integrated models.

Related to scaled experiments is the challenge for accurate identification of hydrodynamic viscous drag coefficients. While already procedures exist to calibrate these coefficients at model scale, a common procedure for the upscaling of the drag coefficients to the real scale is yet to be agreed on.

With more and more available large-scale prototypes, instrumentation techniques, monitoring tools and methods for failure prediction and structural health monitoring will need to be developed. Such monitoring may also enable statistical and data science based approaches towards design.

For a reduction of uncertainty in the design process, a reliable prediction of extreme loads and probabilistic design models will be of importance. In this context, uncertainties in input data are a key limitation for the accuracy of numerical results, regardless of the model's inherent accuracy. Here mainly uncertainties in metocean conditions and soil data are relevant, see e.g. [89], as well as uncertainty in extrapolation methods for extreme events ([90]). Furthermore, differences of the numerical model to the as-built structure are also an important aspect. To address such uncertainties research in model updating and digital twin solutions for offshore wind applications is increasing, see e.g. [91].

Looking further ahead, models encompassing multiple disciplines and large temporal and spatial length scales (such as a fluid structure CFD-FEM models simultaneously resolving the lengthscales of the substructure hull, boundary layer, and the mesoscale regional climate), are likely to remain both practically impossible and impractical for the foreseeable future. This is due to the extensive computational requirements needed for such models, but also due to them not being necessary to obtain sufficiently accurate design load predictions. Often the couplings and interactions between different scales and disciplines are sufficiently small such that a decoupling of models is perfectly acceptable, depending on the quantities the designer is interested in. For example the influence of an offshore substructure on the mesoscale wave climate of a region can be neglected when defining the metocean conditions, as well as (to a lesser extent) the influence of hydroelasticity of a essentially rigid

large concrete floating structure is likely to not influence the hydrodynamic forces on the structure itself to any relevant extent. Here reasonable scientific and engineering judgement is key in order to determine the level of model fidelity required for a specific purpose. This is why the different discussed models in this chapter, ranging from simple semi-empirical methods, over medium-complexity potential flow methods to most complex CFD models, all have their different areas for application and benefit from incremental improvements within their respective boundary conditions.

References

- [1] Faltinsen OM, Newman JN, Vinje T. Nonlinear wave loads on a slender vertical cylinder. *J Fluid Mech.* 1995;289:179–198.
- [2] Newman JN. *Marine Hydrodynamics*. Cambridge, USA: MIT Press; 1977.
- [3] Journée JMJ, Massie WW. *Offshore Hydromechanics*. 1st ed. Delft University of Technology; 2001. Available from: https://ocw.tudelft.nl/wp-content/uploads/OffshoreHydromechanics_Journee_Massie.pdf.
- [4] Muskulus M, Schafhirt S. Design optimization of wind turbine support structures — a review. *J Ocean Wind Energy.* 2014;1:12–22.
- [5] Strach-Sonsalla M, Muskulus M. Prospects of floating wind energy. *Int J Offshore Polar Engng.* 2016;26:81–87.
- [6] Tran TT, Kim DH. A CFD study of coupled aerodynamic-hydrodynamic loads on a semisubmersible floating offshore wind turbine. *Wind Energy*;21(1):70–85. Available from: <https://onlinelibrary.wiley.com/doi/abs/10.1002/we.2145>.
- [7] de Klerk D, Rixen DJ, Voormeeren SN. General framework for dynamic substructuring — history, review, and classification of techniques. *AIAA Journal.* 2008;46:1169–81.
- [8] Matha D, Pérez Moran G, Müller K, et al. Comparative analysis of industrial design methodologies for fixed-bottom and floating wind turbines. In: *Proceedings of the ASME 35th International Conference on Ocean, Offshore and Arctic Engineering*. Busan, Korea; 2016. .
- [9] Müller K, Lemmer F, Borisade F, et al. LIFES50+ D7.4 State-of-the-art FOWT design practice and guidelines. University of Stuttgart; 2015. Available from: http://lifes50plus.eu/wp-content/uploads/2015/11/GA_640741_LIFES50_D7.4.pdf.
- [10] James R, Costa Ros M. *Floating offshore wind: Market and technology review*. The Carbon Trust; 2015. Available from: <http://www.carbontrust.com/media/670664/floating-offshore-wind-market-technology-review.pdf>.
- [11] Hasselmann S, Hasselmann K, Bauer E, et al. The WAM model — a third generation ocean wave prediction model. *J Phys Oceanogr.* 1988;15:1775–810.
- [12] Tolman HL. User manual and system documentation of WAVEWATCH-III version 1.18. NOAA / NWS / NCEP / OMB Technical Note 166; 1999.
- [13] Ris RC, Booij N, Holthuijsen LH. A third-generation wave model for coastal regions, Part II, Verification. *J Geophys Res.* 1999;104:7667–81.

- [14] Holthuijsen LH. Waves in oceanic and coastal waters. Cambridge University Press; 2007.
- [15] Berkhoff JCW. Computation of combined refraction diffraction. In: Proc. 13th Int. Coast. Eng. Conf.; 1972. p. 471–90.
- [16] Blumberg AF, Mellor GL. In: A description of a three-dimensional coastal ocean circulation model; 1987. p. 208.
- [17] McCormick ME. Ocean Engineering Mechanics. Cambridge University Press; 2010.
- [18] Ochi MK. Ocean waves — the stochastic approach. Cambridge University Press; 1998.
- [19] Shinozuka M, Jan CM. Digital simulation of random processes and its applications. J Sound Vibration. 1972;25:111–128.
- [20] Dean RG, Dalrymple RA. Water wave mechanics for engineers and scientists. World Scientific; 1991.
- [21] Chakrabarti SK. Hydrodynamics of offshore structures. WIT Press; 1987.
- [22] Wheeler JD. Method for calculating forces produced by irregular waves. J Petroleum Tech. 1970;3:359–367.
- [23] Lupton R. Frequency-domain modelling of floating wind turbines. University of Cambridge; 2014. Available from: <https://www.repository.cam.ac.uk/bitstream/handle/1810/252880/thesis.pdf>.
- [24] Lemmer F. Low-Order Modeling , Controller Design and Optimization of Floating Offshore Wind Turbines. University of Stuttgart; 2018.
- [25] Dean RG. Stream function representation of nonlinear ocean waves. J Geophys Res. 1965;70:4561–72.
- [26] Lin P. Numerical modeling of water waves. Taylor & Francis; 2008.
- [27] Nichols BD, Hirt CW, Hotchkiss RS. SOLA-VOF: A solution algorithm for transient fluid flow with multiple free-boundaries; 1980.
- [28] Osher S, Sethian JA. Fronts propagating with curvature-dependent speed-algorithms based on Hamilton-Jacobi formulations. J Comput Phys. 1988;79:12–49.
- [29] Spalart PR, Allmaras SR. A one-equation turbulence model for aerodynamic flows; 1992.
- [30] Dalrymple RA, Rogers BD. Numerical modeling of water waves with the SPH method. Coastal Eng. 2006;53:141–147.
- [31] McCowan J. On the highest wave of permanent type. Philos Mag J Sci. 1894;5:351–8.
- [32] Battjes JA. Surf similarity parameter. In: Proc. 14th Int. Conf. Coast Eng.; 1974. p. 69–85.
- [33] Wienke J, Oumeraci H. Breaking wave impact force on a vertical and inclined slender pile — theoretical and large-scale model investigations. Coast Eng. 2005;52:435–62.
- [34] Tu Y, Muskulus M, Arntsen A. Experimental analysis of slamming load characteristics for truss structures in offshore wind applications. J Ocean Wind Energy. 2015;2:138–145.

- [35] Tu Y, Cheng Z, Muskulus M. A global slamming force model for offshore wind jacket structures. *Marine Structures*. 2018;60:201–217.
- [36] Naess A, Moan T. *Stochastic dynamics of marine structures*. Cambridge University Press; 2013.
- [37] Tromans PS, Anaturk AR, Hagemeyer P. A new model for the kinematics of large ocean waves — application as a design wave. In: *Proc. First (1991) International Offshore and Polar Engineering Conference*; 1991. p. 64–71.
- [38] Beirlant J, Goegebeur Y, Teugels J, et al. *Statistics of extremes: theory and applications*. John Wiley & Sons; 2004.
- [39] De Michele C, Salvadori G, Passoni G, et al. A multivariate model of sea storms using copulas. *Coastal Eng*. 2007;54:734–751.
- [40] Haver S, Winterstein SR. Environmental contour lines: A method for estimating long term extremes by a short term analysis. *Transactions, Society of Naval Architects and Marine Engineers*. 2009;116:116–27.
- [41] Young IR. A review of the sea state generated by hurricanes. *Marine Structures*. 2003;16:201–18.
- [42] Han T, McCann G, Mcke TA, et al. How can a wind turbine survive a tropical cyclone? *Renewable Energy*. 2014;70:3–10.
- [43] Kim E, Manuel L. On the simulation of wind, waves and currents during hurricane Sandy for assessing the performance of jacket-supported offshore wind turbines. In: *Proc. 35th Int. Conf. OMAE*; 2016. p. 54656:1–8.
- [44] Forristall GZ, Ewans KC. Worldwide measurement of directional wave spreading. *J Atmos Oceanic Tech*. 1998;15:440–69.
- [45] Horn JT, Krokstad JR, Amdahl J. Long-term fatigue damage sensitivity to wave directionality in extra-large monopile foundations. *Proc IMechE Part M: J Engineering for the Maritime Environment*. 2018;232:37–49.
- [46] Faltinsen OM. *Sea Loads On Ships And Offshore Structures*. Cambridge University Press; 1993.
- [47] Sarpkaya T. *Wave Forces on Offshore Structures*. 1st ed. Cambridge University Press; 2010.
- [48] Cummins W. The impulse response function and ship motion. In: *Proceedings of the Symposium on Ship Theory*. Hamburg, Germany; 1962. .
- [49] Ogilvie TF. Recent progress toward the understanding and prediction of ship motions. In: *Proceedings of the Fifth Symposium on Naval Hydrodynamics*. Bergen, Norway; 1964. .
- [50] Jonkman J, Robertson A, Hayman G. *HydroDyn user’s guide and theory manual*. Boulder, USA: National Renewable Energy Laboratory; 2014. Available from: https://nwtc.nrel.gov/system/files/HydroDyn_Manual.0.pdf.
- [51] Pérez T, Fossen T. A matlab toolbox for parametric identification of radiation-force models of ships and offshore structures. *Journal of Modeling, Identification and Control*. 2009;30(1):1–15. Available from: <http://www.mic-journal.no/ABS/MIC-2009-1-1.asp>.
- [52] Duarte T, Sarmiento A, Alves M, et al. State-space realization of the wave-radiation force within FAST. In: *Proceedings of the ASME 32nd Inter-*

- national Conference on Ocean, Offshore and Arctic Engineering. Nantes, France; 2013. Available from: <http://www.nrel.gov/docs/fy13osti/58099.pdf>.
- [53] Taghipour R, Pérez T, Moan T. Hybrid frequency-time domain models for dynamic response analysis of marine structures. *Ocean Engineering*. 2008;35(7):685–705. Available from: <http://linkinghub.elsevier.com/retrieve/pii/S0029801807002363>.
- [54] Yu Z, Falnes J. State-space modelling of a vertical cylinder in heave. *Applied Ocean Research*. 1995;17(5):265–275. Available from: <http://www.marinecontrol.org/References/papers/YuFalnes1995.pdf>.
- [55] Lemmer F, Raach S, Schlipf D, et al. Parametric wave excitation model for floating wind turbines. *Energy Procedia*. 2016;94:290–305. Available from: <http://dx.doi.org/10.1016/j.egypro.2016.09.186>.
- [56] Schlipf D, Sandner F, Raach S, et al. Nonlinear model predictive control of floating wind turbines. In: *Proceedings of the 23rd International Ocean and Polar Engineering Conference*. Anchorage, USA; 2013. p. 440–447. Available from: <http://dx.doi.org/10.18419/opus-3908>.
- [57] Schlipf D, Simley E, Lemmer F, et al. Collective pitch feedforward control of floating wind turbines using Lidar. *Journal of Ocean and Wind Energy*. 2015;2(4):223–230. Available from: <http://www.isope.org/publications/jowe/jowe-02-4/joweNov15.htm>.
- [58] Langley RS. On the time domain simulation of second order wave forces and induced responses. *Applied Ocean Research*. 1986;8(3):134–143.
- [59] Newman JN. Second-order, slowly-varying forces on vessels in irregular waves. In: *Proceedings of International Symposium on Dynamics of Marine Vehicles and Structures in Waves*. London, UK; 1974. .
- [60] Duarte T, Sarmiento A, Jonkman J. Effects of second-order hydrodynamic forces on floating offshore wind turbines. In: *Proceedings of the AIAA SciTech*. National Harbor, USA; 2014. Available from: <http://www.nrel.gov/docs/fy14osti/60966.pdf>.
- [61] Standing RG, Brendling WJ, Wilson D. Recent developments in the analysis of wave drift forces, low-frequency damping and response. In: *Proceedings of the Offshore Technology Conference*. Houston, USA; 1987. .
- [62] NWTC. NWTC information portal (FAST v8); 2016. Available from: <https://nwtc.nrel.gov/FAST8>.
- [63] Morison JR. *The force distribution exerted by surface waves on piles*. Berkeley, USA: University of California, Institute of Engineering Research; 1953.
- [64] Sarpkaya T, Isaacson M. *Mechanics of Wave Forces on Offshore Structures*. Van Nostrand Reinhold Co.; 1981.
- [65] Östergaard C, Schellin TE. Comparison of experimental and theoretical wave actions on floating and compliant offshore structures. *Applied Ocean Research*. 1987;9(4).
- [66] Robertson A, Jonkman J, Vorpahl F, et al. Offshore Code Comparison Collaboration Continuation within IEA Wind Task 30: Phase II results regarding a floating semisubmersible wind system. In: *Proceedings of the ASME 33rd*

- International Conference on Ocean, Offshore and Arctic Engineering. San Francisco, USA; 2014. .
- [67] Stewart G, Muskulus M. A Review and Comparison of Floating Offshore Wind Turbine Model Experiments. *Energy Procedia*. 2016;94:227 – 231. 13th Deep Sea Offshore Wind R&D Conference, EERA Deep-Wind'2016. Available from: <http://www.sciencedirect.com/science/article/pii/S1876610216309146>.
- [68] Luan C, Gao Z, Moan T. Development and verification of a time-domain approach for determining forces and moments in structural components of floaters with an application to floating wind turbines. *Marine Structures*. 2017;51:87–109. Available from: <http://dx.doi.org/10.1016/j.marstruc.2016.10.002>.
- [69] Borg M, Bredmose H, Hansen AM. Elastic deformations of floaters for offshore wind turbines: dynamic modelling and sectional load calculations. In: *Proceedings of the ASME 36th International Conference on Ocean, Offshore and Arctic Engineering*. Trondheim, Norway; 2017. .
- [70] Buchner B, Garcia JLC. Design aspects of green water loading on FPSOs. In: *Proc. 22nd Int. Conf. OMAE*; 2003. p. 37162:1–11.
- [71] Masciola M, Jonkman J, Robertson A. Implementation of a multisegmented, quasi-static cable model. 2013 01;p. 315–322.
- [72] Hall M, Buckham B, Crawford C. Evaluating the importance of mooring line model fidelity in floating offshore wind turbine simulations. *Wind Energy*;17(12):1835–1853. Available from: <https://onlinelibrary.wiley.com/doi/abs/10.1002/we.1669>.
- [73] Masciola M, Jonkman J, Robertson A. Extending the Capabilities of the Mooring Analysis Program: A Survey of Dynamic Mooring Line Theories for Integration into FAST: Preprint;.
- [74] Lopez-Pavon C, Souto-Iglesias A. Hydrodynamic coefficients and pressure loads on heave plates for semi-submersible floating offshore wind turbines — a comparative analysis using large scale models. *Renewable Energy*. 2015;81:864–81.
- [75] Zhang S, Ishihara T. Numerical study of hydrodynamic coefficients of multiple heave plates by large eddy simulations with volume of fluid method. *Ocean Engng*. 2018;163:583–98.
- [76] Blevins RD. *Flow-induced vibration*. Krieger Publishing; 2001.
- [77] Chakrabarti S. Physical Model Testing of Floating Offshore Structures. In: *Proceedings of the Dynamic Positioning Conference*; 1998. .
- [78] Grue J, Huseby J. Higher-harmonic wave forces and ringing of vertical cylinders. *Appl Ocean Res*. 2002;24:203–214.
- [79] Bachynski EE, Moan T. Ringing loads on tension leg platform wind turbines. *Ocean Eng*. 2014;84:237–248.
- [80] Johannessen TB. Nonlinear superposition methods applied to continuous ocean wave spectra. *J OMAE*. 2012;134:011302:1–14.
- [81] Németh AA, Hulscher SJMH, de Vriend HJ. Modelling sand wave migration in shallow shelf seas. *Continental Shelf Res*. 2002;22:2795–2806.

- [82] Whitehouse RJS, Harris JM, Sutherland J, et al. The nature of scour development and scour protection at offshore windfarm foundations. *Marine Pollution Bull.* 2011;62:73–88.
- [83] De Vos L, De Rouck J, Troch P, et al. Empirical design of scour protections around monopile foundations, Part 1, Static approach. *Coastal Eng.* 2011;58:540–553.
- [84] Depina I, Le TMH, Eiksund G, et al. Behavior of cyclically loaded monopile foundations for offshore wind turbines in heterogeneous sands. *Computers and Geotechnics.* 2015;65:266–277.
- [85] BSI. Petroleum and natural gas industries arctic offshore structures (BS EN ISO 19906:2010). British Standards Institution; 2010.
- [86] Hendrikse H, Metrikine A. Interpretation and prediction of ice induced vibrations based on contact area variation. *Int J Solids Struct.* 2015;75–76:336–48.
- [87] Ashby M, Palmer A, Thouless M, et al. Nonsimultaneous failure and ice loads on arctiv structures. In: *Offshore Technology Conference*; 1986. .
- [88] Seidel M, Hendrikse H. Analytical assessment of sea ice-induced frequency lock-in for offshore wind turbine monopiles. *Marine Structures.* 2018;60:87–100.
- [89] Bitner-Gregersen EM, Dong S, Fu T, et al. Sea state conditions for marine structures’ analysis and model tests. *Ocean Engineering.* 2016;119:309 – 322. Available from: <http://www.sciencedirect.com/science/article/pii/S0029801816300105>.
- [90] Lott S, Cheng PW. Load extrapolations based on measurements from an offshore wind turbine at alpha ventus. *Journal of Physics: Conference Series.* 2016;753(7):072004. Available from: <http://stacks.iop.org/1742-6596/753/i=7/a=072004>.
- [91] Erikstad S. *Merging Physics, Big Data Analytics and Simulation for the Next-Generation Digital Twins*; 2017.